

**$\alpha$ -decay spectra of odd nuclei using the effective Skyrme interaction**

D. E. Ward,\* B. G. Carlsson, and S. Åberg

*Mathematical Physics, LTH, Lund University, PO Box 118, S-22100 Lund, Sweden*

(Received 19 May 2015; published 20 July 2015)

**Background:** For nuclei heavier than  $^{208}\text{Pb}$   $\alpha$  decay is a dominating decay mode.  $\alpha$  decay of odd nuclei can give spectroscopic information because different states in the daughter nucleus can be populated in the decay.

**Purpose:** To explore and test microscopic descriptions of  $\alpha$  decay of odd nuclei based on self-consistent models with effective nuclear interactions. To predict the hindrance of  $\alpha$  decay of odd- $A$  superheavy nuclei.

**Methods:** We apply the method of our previous work [D. E. Ward, B. G. Carlsson, and S. Åberg, *Phys. Rev. C* **88**, 064316 (2013)] to the case of odd- $A$  near-spherical nuclei. The Skyrme effective interaction SLy4 is used. Starting from the obtained Hartree-Fock-Bogoliubov vacuum and quasiparticle excitations, the  $\alpha$ -particle formation amplitude is calculated giving the decay rates and hindrance of different  $\alpha$ -decay channels.

**Result:** The calculated relative decay rates show good agreement with available data. The hindrance of decay channels where the odd nucleon changes orbital is reasonably described by the microscopic calculation. Several hindered ground-state decays of superheavy nuclei are predicted, implying possible  $\alpha$ - $\gamma$  coincidences.

**Conclusions:** The approach offers a practical method of making quantitative predictions for the relative hindrance of different  $\alpha$ -decay channels.

DOI: [10.1103/PhysRevC.92.014314](https://doi.org/10.1103/PhysRevC.92.014314)

PACS number(s): 23.60.+e, 21.60.Jz, 21.10.Tg, 27.90.+b

**I. INTRODUCTION**

The  $\alpha$ -decay spectra of odd nuclei show more complexity than for even nuclei. Several  $\alpha$ -decay channels with different  $Q_\alpha$  values and partial half-lives are often observed. By comparing the partial half-life with the corresponding half-life for an even-even nucleus one observes a hindrance of certain decay channels—an increase in partial half-life not attributable to energetics. The hindrance arises from different structure of the mother nucleus and daughter nucleus states, and can make decays populating excited states in the daughter nucleus more probable than the more energetic decay populating the ground state. Consequently,  $\alpha$  decay of odd nuclei provides spectroscopic information from the  $\alpha$ -decay fragmentation, as well as from  $\gamma$  decay following  $\alpha$  decay to excited states.

$\alpha$  decay is a dominating decay mode in many heavy and superheavy nuclei (SHN). The  $\alpha$ -decay half-lives are important for determining which SHN are the longest lived in a proposed island of stability [1–3]. In the case of odd SHN the half-life can be enhanced by hindrance. Information on the level structure of the heaviest elements can provide important constraints on effective interactions. One way to obtain this structure data is through  $\alpha$ - $\gamma$ -spectroscopy experiments, where the subsequent  $\gamma$  decays of low-lying excited states populated by the  $\alpha$  decay are measured; see, e.g., [4]. In recent experiments [5], one has also detected x rays that allows for the proton number of the daughter nucleus to be determined. This calls for accurate theoretical predictions for the hindrance of the  $\alpha$  decays of SHN.

Empirically the hindrance shows some regularity [6,7], where different hindrance factors are associated with different classes of decay scenarios. To fully describe the hindrance calls for a microscopic description, where the nuclear structure of

the mother, daughter, and  $\alpha$  nuclei are explicitly considered. Already in early microscopic calculations using simple shell-model wave functions, some of the variation in the relative decay rates of odd-mass nuclei near  $^{208}\text{Pb}$  could be explained [8–10]. Microscopic calculations using a BCS description [11] offered an interpretation of hindrance in terms of loss of pairing enhancement, and differences in single-particle wave functions for odd- $A$   $\alpha$  decay.

Skyrme-Hartree-Fock-Bogoliubov (SHFB) and other self-consistent mean-field models are applicable throughout the chart of nuclides [12]. The reasonable description of bulk ground-state properties of large numbers of nuclei offered by these models motivates the extrapolation to unknown regions of nuclei. Indeed, SHFB models have been applied extensively to predict different properties of superheavy nuclei [3,13,14]. Such self-consistent models thus provide an excellent basis for the simultaneous description of the structure of different nuclear states and the  $\alpha$  decay.

In our previous work [15] we applied a SHFB nuclear structure model in microscopic  $\alpha$ -decay calculations for near-spherical even-even nuclei. The obtained  $\alpha$ -particle formation amplitudes in the nuclear surface, sensitive to the tail of the nuclear wave function, were shown to be converged with respect to the size of the large spherical oscillator basis used. The obtained  $\alpha$ -decay half-lives were too long, but relative values could be well described. In this work we investigate if a similar good agreement for relative decay rates is obtained for the case of near-spherical odd- $A$   $\alpha$ -decaying nuclei. We also microscopically test the description of hindrance of different categories of  $\alpha$ -decay channels, and to what extent simple classifications or selection rules, based on the spin and parity of the mother and daughter nucleus, can be used to determine the hindrance factor. The approach is then applied to make predictions for the  $\alpha$  decay of odd- $A$  superheavy nuclei, specifically the hindrance of the decay populating the daughter nucleus ground state.

\*daniel.ward@matfys.lth.se

A brief review of the formalism and calculation method is presented in Sec. II. Available experimental data to be compared with the results of calculations and classification of  $\alpha$ -decay channels is detailed in Sec. III. The results for known odd- $A$   $\alpha$  decays and a detailed quantitative comparison of the obtained results with the data is presented in Sec. IV. Sensitivity of the predicted hindrance to the pairing properties of the employed SHFB model is investigated in Sec. V. Predictions of the ground-state-to-ground-state  $\alpha$  decay of superheavy nuclei, and possibilities of  $\alpha$  decay to excited states, are presented in Sec. VI. A summary of the results and an outlook is presented in Sec. VII.

## II. METHOD

We employ the same general formalism used in the previous work [15] to describe the  $\alpha$ -decay rates. In that work several aspects of the formalism and the approximations involved are discussed. This microscopic approach to  $\alpha$  decay, based on  $R$ -matrix theory, is reviewed in [16,17]. Here we briefly review the parts relevant for the current work, focusing on the additional aspects relevant for the treatment of odd nuclei that do not arise in the even case.

In Sec. II A expressions for the nuclear wave functions are provided. The decay width is treated in Sec. II B and the calculation of the  $\alpha$ -particle formation amplitude in Sec. II C. The application of the method is detailed in Sec. II D. Details on the  $\alpha$ -particle wave function and the two-particle transfer amplitudes are provided in two appendixes.

### A. Nucleus wave functions

The present study is restricted to near-spherical odd- $A$  nuclei. We consider the simplest extension from the even-even case treated in [15] by describing the odd nucleus as a one-quasiparticle excitation  $\beta^\dagger$  on top of the HFB vacuum. For an  $\alpha$ -decaying odd-proton nucleus the mother ( $M$ ) and daughter ( $D$ ) states are

$$|M; k_M I_M M_M\rangle = (\beta_{k_M I_M M_M}^{(M)\dagger} |M_0^\pi\rangle) \otimes |M_0^v\rangle, \quad (1)$$

$$|D; k_D I_D M_D\rangle = (\beta_{k_D I_D M_D}^{(D)\dagger} |D_0^\pi\rangle) \otimes |D_0^v\rangle, \quad (2)$$

where  $|M_0^{\pi/v}\rangle$  ( $|D_0^{\pi/v}\rangle$ ) is the proton or neutron part of the spherically symmetric HFB vacuum for the mother (daughter) nucleus  $|M_{00}\rangle$  ( $|D_{00}\rangle$ ).  $I_M$  ( $I_D$ ) and  $M_M$  ( $M_D$ ) is the spin and spin projection of the mother (daughter) nucleus and  $k_M$  ( $k_D$ ) labels the quasiparticle orbital. The vacuum  $|M_{00}\rangle$  ( $|D_{00}\rangle$ ) is obtained by solving the HFB equations in a spherical oscillator basis, with the average particle numbers constrained to those of the odd nucleus.

The  $\alpha$ -particle formation amplitudes for even-even nuclei obtained in microscopic SHFB calculations show a large sensitivity to the pairing strength, but appears relatively insensitive to which Skyrme effective interaction is used [15,18]. As long as the variation of the pairing properties with proton and neutron number are similar, we expect different Skyrme parametrizations to give similar predictions for even nuclei. For the odd- $A$  nuclei considered here the shell structure enters more directly in the  $\alpha$ -decay widths through the different

quasiparticles. We use the well-tested Skyrme interaction SLy4 [19], which gives a reasonable description of the shell structure around  $^{208}\text{Pb}_{126}$ . SLy4 was also applied in large-scale calculations for SHN, giving good agreement between the obtained  $Q_\alpha$  values and available experimental data [13,14].

The SLy4 particle-hole interaction is combined with the pairing recipes ‘‘volume pairing’’ and ‘‘surface pairing’’ used in [15]. We also employ a pairing of mixed surface and volume type, ‘‘mixed pairing’’ that will be used in the calculations for SHN. The strength of the mixed pairing is tuned to reproduce experimental odd-even mass differences for  $_{100}\text{Fm}_{150-159}$  isotopes and  $_{94-105}\text{X}_{150}$  isotones. This is achieved by setting the mixed pairing force strength to 90% of the default values for SLy4 in the code presented in Ref. [20]. The Lipkin-Nogami method for approximate particle number projection is used to avoid the collapse of pairing, that otherwise occurs for magic nuclei.

The HFB wave functions are obtained using a modified version of the program HOSPHE [21]. All major oscillator shells up to  $N_{\text{max}} = 30$  are included in the harmonic oscillator basis. Coulomb exchange is treated in the Slater approximation.

### B. Decay width

The decaying mother nucleus can be described as an exponentially decaying Gamow state. This state can have several decay channels  $k$ ; here we only consider those corresponding to a fragmentation of the nucleus into an  $\alpha$  particle and a daughter state of the type (2). As the different daughter states are orthogonal, the decay width can be written,

$$\Gamma = \sum_k \Gamma_k, \quad (3)$$

where  $\Gamma_k$  is the decay width for channel  $k$ . The decay width can be decomposed in partial waves,

$$\Gamma_k = \sum_{L_\alpha} \Gamma_{kL_\alpha}, \quad (4)$$

where  $\Gamma_{kL_\alpha}$  is the partial width corresponding to the fragmentation  $k$  and  $\alpha$ -particle angular momentum  $L_\alpha$ . When the  $\alpha$  particle and the daughter nucleus are well separated they only interact through the Coulomb repulsion, which for the spherical nuclei studied in this work is isotropic. The radial part of the relative motion of the two fragments in a given partial wave can then be described by an outgoing Coulomb wave function. This leads to the  $R$ -matrix expression [16,17] for the decay width,

$$\Gamma_{kL_\alpha}^{(R)}(r_c) = 2\gamma_{kL_\alpha}^2(r_c) P_{L_\alpha}(Q_{\alpha k}, r_c), \quad (5)$$

where  $P_{L_\alpha}(Q_{\alpha k}, r_c)$  is the Coulomb penetrability and  $\gamma_{kL_\alpha}^2(r_c)$  is the reduced width.  $Q_{\alpha k}$  is the  $Q$  value for the decay into the fragments  $k$ , and  $r_c$  is a matching radius which should be chosen beyond the range of interfragment nuclear forces.

The Coulomb penetrability  $P_{L_\alpha}(Q_{\alpha k}, r_c)$  depends on the magnitude of the Coulomb repulsion, proportional to the number of protons in the daughter nucleus.  $P_{L_\alpha}$  takes into account the centrifugal barrier from the angular momentum  $L_\alpha$  and depends on the linear momentum of the relative motion, which depends on  $Q_\alpha$ . It is highly energy dependent because

of the tunneling through the combined Coulomb and centrifugal barrier. The reduced width contains the microscopic overlap of initial and fragment states, and is defined as

$$\gamma_{kL_\alpha}^2(r_c) = \frac{\hbar^2}{2\mu r_c} r_c^2 f_{kL_\alpha}^2(r_c), \quad (6)$$

where  $\mu$  is the reduced mass,  $f_{kL}(r)$  is the formation amplitude, and  $r$  is the separation between daughter and  $\alpha$  particle centers of mass. The choice of the matching radius  $r = r_c$  is described in Sec. II D.

### C. Formation amplitude

The formation amplitude is given by

$$f_{kL_\alpha}(r) = \sqrt{8} g_{kL_\alpha}(2r), \quad (7)$$

where  $g_{kL_\alpha}$  is defined as the overlap between the mother nucleus  $\Psi_{I_M M_M}^{(M)}$ , and the  $\alpha$  cluster  $\Phi_{L_\alpha}^{(C)}$ , coupled to the daughter nucleus  $\Psi_k^{(D)}$ ,

$$g_{kL_\alpha}(R'_\alpha) = \int dX_D d\xi_\alpha d\mathbf{R}_\alpha \mathcal{A}_{D\alpha} [\Psi_k^{(D)}(X_D), \Phi_{L_\alpha}^{(C)}(R'_\alpha; \xi_\alpha, \mathbf{R}_\alpha)]_{I_M M_M}^* \Psi_{I_M M_M}^{(M)}(X_M), \quad (8)$$

where  $\mathbf{R}_\alpha$  and  $\xi_\alpha \equiv (\mathbf{r}_\pi, \mathbf{r}_\nu, \mathbf{r}_\alpha)$  are the standard Jacobi coordinates (A2),  $X_D$ , and  $X_M = \{\mathbf{r}_1, \mathbf{r}_2, \mathbf{r}_3, \mathbf{r}_4, X_D\}$  are the laboratory coordinates for the daughter and mother nucleus. The symbol  $\mathcal{A}_{D\alpha}$  implies antisymmetrization of the daughter and  $\alpha$  particle. The cluster function  $\Phi_{L_\alpha M_\alpha}^{(C)}$  is defined,

$$\Phi_{L_\alpha M_\alpha}^{(C)}(R'_\alpha; \mathbf{r}_\pi, \mathbf{r}_\nu, \mathbf{r}_\alpha, \mathbf{R}_\alpha) = \Phi_{00}^{(\alpha)}(\mathbf{r}_\pi, \mathbf{r}_\nu, \mathbf{r}_\alpha) \frac{\delta(R_\alpha - R'_\alpha)}{R_\alpha^2} Y_{L_\alpha M_\alpha}(\hat{R}_\alpha), \quad (9)$$

where  $\Phi_{00}^{(\alpha)}(\mathbf{r}_\pi, \mathbf{r}_\nu, \mathbf{r}_\alpha)$  is the standard intrinsic  $\alpha$ -particle wave function (A1).

The  $\alpha$ -cluster function is expanded in a basis,

$$|\Phi_{L_\alpha M_\alpha}^{(C)}(R'_\alpha)\rangle = \sum_{i < j} \sum_{k < l} |ijkl\rangle \langle ijkl | \Phi_{L_\alpha M_\alpha}^{(C)}(R'_\alpha)\rangle, \quad (10)$$

where  $|ijkl\rangle = a_{\pi i}^\dagger a_{\pi j}^\dagger |0^\pi\rangle \otimes a_{\nu k}^\dagger a_{\nu l}^\dagger |0^\nu\rangle$  is a two-proton plus two-neutron state, and the overlap is given by

$$\langle ijkl | \Phi_{L_\alpha M_\alpha}^{(C)}(R'_\alpha)\rangle = \int d\mathbf{R}_\alpha d\xi_\alpha \mathcal{A}_{12} \{\phi_i(\mathbf{r}_1) \phi_j(\mathbf{r}_2)\}^* \mathcal{A}_{34} \{\phi_k(\mathbf{r}_3) \phi_l(\mathbf{r}_4)\}^* \Phi_{L_\alpha M_\alpha}^{(C)}(R'_\alpha; \xi_\alpha, \mathbf{R}_\alpha). \quad (11)$$

Inserting expansion (10) into (8), we get the expression

$$g_{L_\alpha}(R'_\alpha) = \sum_{M_D M_\alpha} C_{I_D M_D L_\alpha M_\alpha}^{I_M M_M} \sum_{i < j} \sum_{k < l} \langle ijkl | \Phi_{L_\alpha M_\alpha}^{(C)}(R'_\alpha)\rangle^* \langle D; k_D I_D M_D | a_{\nu l} a_{\nu k} a_{\pi j} a_{\pi i} | M; k_M I_M M_M \rangle, \quad (12)$$

containing a four-particle transfer amplitude. Using the expressions for the transfer amplitudes (B5), (B8) in Appendix B and transforming [22] to the Jacobi coordinates (A2) gives

$$g_{L_\alpha}(R'_\alpha) = \delta_{I, I_D} \delta_{L_\alpha, 0} F_{k_D, k_M}^\pi g_0^F(R'_\alpha) - \frac{1 + (-1)^{l_M + l_D - L_\alpha}}{2} g_{L_\alpha}^H(R'_\alpha), \quad (13)$$

where  $F_{k_D, k_M}^\pi$  is given by (B9) and  $g_0^F$  is the formation amplitude for the HFB vacua  $|M_{00}\rangle$  and  $|D_{00}\rangle$  [15]. The second term is given by

$$\begin{aligned} g_{L_\alpha}^H(R'_\alpha) &= \langle D_0^\pi | M_0^\pi \rangle \langle D_0^\nu | M_0^\nu \rangle \frac{1}{2} \sqrt{2I_D + 1} \sqrt{2L_\alpha + 1} (-1)^{l_M + L_\alpha + \frac{1}{2} + I_D} \begin{Bmatrix} l_D & l_M & L_\alpha \\ I_M & I_D & \frac{1}{2} \end{Bmatrix} \sum_{l_\nu j_\nu} \frac{2j_\nu + 1}{\sqrt{2l_\nu + 1}} \sum_{n_3 \leq n_4} (2 - \delta_{n_3 n_4}) \mathcal{K}_{n_3 n_4}^{(DM)\nu, l_\nu j_\nu} \\ &\times \sum_{nn'} H_{(nl_M), k_M; (n'l_D), k_D}^\pi \sum_{N_{12}} \langle N_{12} L_\alpha, n_{12} 0; L_\alpha | n l_M, n' l_D; L_\alpha \rangle \sum_{N_{34}} \langle N_{34} 0, n_{34} 0; 0 | n_3 l_\nu, n_4 l_\nu; 0 \rangle \\ &\sum_{N_\alpha n_\alpha} \langle N_\alpha L_\alpha, n_\alpha 0; L_\alpha | N_{12} L_\alpha, N_{34} 0; L_\alpha \rangle I_{n_{12}}^{(b, b_\alpha)} I_{n_{34}}^{(b, b_\alpha)} I_{n_\alpha}^{(b, b_\alpha)} R_{N_\alpha L_\alpha}^{(b)}(R'_\alpha), \end{aligned} \quad (14)$$

where the  $H_{(nl_M), k_M; (n'l_D), k_D}^\pi$  coefficients are given by (B10) and

$$I_n^{(b, b_\alpha)} = \int r^2 dr R_{00}^{(b_\alpha)*}(r) R_{n0}^{(b)}(r). \quad (15)$$

$R_{nl}^{(b)}(r)$  is here the radial part of a spherical oscillator wave function with  $n$  nodes and angular momentum  $l$ , and  $b$  denotes the oscillator length used for the basis. The overlap of HFB vacua  $\langle D_0^\pi | M_0^\pi \rangle$  is calculated in the same way as in the previous

article [15]. A similar expression is obtained in the case of odd neutron states.

#### D. Application

##### 1. $Q$ values and matching radius

As the Coulomb penetrability is highly energy dependent, we calculate the decay width (5) using the experimental  $Q_\alpha$  value for the decay channel  $Q_{\alpha k}^{\text{exp}}$  unless stated otherwise. The matching radius  $r_c$  is chosen as the touching radius  $r_t$  of the daughter and  $\alpha$  particle,

$$r_t = r_0(4^{1/3} + A_D^{1/3}), \quad (16)$$

with  $r_0 = 1.2$  fm, and  $A_D$  the number of nucleons of the daughter nucleus.

##### 2. Phenomenological scaling

In [15] it was found that for  $\alpha$  decay of even nuclei, the adopted model underestimates the absolute values of the decay rates. On the other hand, relative values were found to be in good agreement with experiment. A phenomenological one-parameter rescaling of the calculated decay rates was introduced, so that the variation in decay rates over an extensive region of even-even nuclei could be more easily compared to experiment. Possible reasons for the need of rescaling were discussed in [15] where several extensions that might improve the model, e.g., by increasing the formation amplitudes were listed. Among those is an improved description of correlations. Several calculations for  $^{212}_{84}\text{Po}_{128}$  [23–26] indeed suggest that a mixing of many configurations can lead to a substantial increase in the formation amplitude.

The current approach employs only pairing correlations and gives a surprisingly good agreement for the relative rates for a large number of even-even nuclei [15]. This indicates that the missing formation amplitude is approximately proportional to the amplitude obtained from the SHFB wave functions. In this work the scaling recipe is tested for the case of odd nuclei using the scaling factors determined in our previous study of even-even nuclei. The  $R$ -matrix decay widths for all considered odd (as well as even) nuclei are thus scaled by the constant factor  $\mathcal{S}$ ,

$$\Gamma_k^{\text{th}} = \mathcal{S} \sum_{L_\alpha} \Gamma_{kL_\alpha}^{(R)}(r_t). \quad (17)$$

The constant  $\mathcal{S}$  is given by the reciprocal geometrical average,

$$\mathcal{S} = 10^{-\mathcal{M}_{ee}}, \quad (18)$$

where  $\mathcal{M}_{ee}$  is calculated for 48 ground-state-to-ground-state decays of near-spherical even-even nuclei studied in [15],

$$\mathcal{M}_{ee} = \frac{1}{n} \sum_{i=1}^n \log_{10}(\Gamma_i^{\text{exp}} / \Gamma_i^{(R)}(r_t)). \quad (19)$$

The mean values  $\mathcal{M}_{ee}$  and corresponding standard deviations,

$$\sigma_{ee} = \sqrt{\frac{1}{n-1} \sum_{i=1}^n (\log_{10}(\Gamma_i^{\text{exp}} / \Gamma_i^{(R)}(r_t)) - \mathcal{M}_{ee})^2},$$

for different pairing approaches are summarized in Table I. It is seen that the best mean agreement with experiment is obtained with surface pairing, giving the smallest absolute mean  $|\mathcal{M}_{ee}|$

TABLE I. Logarithm of geometric mean relative errors, and corresponding standard deviations for near-spherical even-even nuclei for three different pairing approaches. For each case results of 50% larger and half pairing strength are also shown.

Model	$\mathcal{M}_{ee}$	$\sigma_{ee}$
SLy4+0.5 $\times$ Vol.P.	−5.136	0.382
SLy4+Vol.P.	−3.854	0.298
SLy4+1.5 $\times$ Vol.P.	−2.498	0.406
SLy4+0.5 $\times$ Mix.P.	−4.987	0.353
SLy4+Mix.P.	−3.422	0.284
SLy4+1.5 $\times$ Mix.P.	−1.568	0.418
SLy4+0.5 $\times$ Surf.P.	−5.144	0.426
SLy4+Surf.P.	−3.233	0.226
SLy4+1.5 $\times$ Surf.P.	−0.127	0.400

as well as the smallest standard deviation. By increasing the surface-pairing interaction strength to a quite unphysical value, the mean comes close to zero ( $\mathcal{M}_{ee} = -0.13$ ), corresponding to on average correct decay widths, but with a quite large spreading  $\sigma_{ee}$ .

### III. EXPERIMENTAL DATA

#### A. Equivalent reduced width

The reduced width (6) depends on the nuclear structure of the mother, daughter, and  $\alpha$  nucleus, with no explicit energy dependence. The Coulomb penetrability on the other hand contains a drastic energy dependence of the tunneling, as well as the effect of the centrifugal barrier, with no dependence on the nuclear structure. To study the influence of nuclear structure on the decay probability, the reduced width is the relevant quantity.

In a typical  $\alpha$ -decay experiment, different  $\alpha$ -decay channels can be identified based on the  $Q_{\alpha k}$  values. The different  $L_\alpha$  partial waves belonging to the same fragmentation  $k$  are usually not resolved. In this case one cannot make a direct comparison of the formation amplitudes for different  $L_\alpha$  values with the experimental data. To compare with experiment, we define a theoretical equivalent reduced width  $\bar{\gamma}_k^2$  by dividing the calculated decay width  $\Gamma_k^{\text{th}}$  with the  $s$ -wave Coulomb penetrability  $P_0(Q_{\alpha k}^{\text{exp}}, r_t)$ ,

$$\bar{\gamma}_k^2(r_t) = \frac{\Gamma_k^{\text{th}}}{2P_0(Q_{\alpha k}^{\text{exp}}, r_t)}. \quad (20)$$

This quantity contains the formation amplitudes of the fragmentation  $k$ . The energy dependence is mostly removed, but the influence of the different centrifugal barriers, for different  $L_\alpha$ , is kept. The corresponding experimental value is obtained from the decay width  $\Gamma_k^{\text{exp}} = \hbar \ln(2) / T_k^{\text{exp}}$ , where  $T_k^{\text{exp}}$  is the observed partial  $\alpha$ -decay half-life, and the measured  $Q_{\alpha k}^{\text{exp}}$ ,

$$\bar{\gamma}_{\text{exp},k}^2(r_t) = \frac{\Gamma_k^{\text{exp}}}{2P_0(Q_{\alpha k}^{\text{exp}}, r_t)}. \quad (21)$$

#### B. Selection of nuclear states

We apply the described theoretical approach to near-spherical odd- $A$   $\alpha$ -emitting nuclei with the calculated

TABLE II. Experimental  $\alpha$ -decay data for odd nuclei indexed with increasing  $A$ .  $Q_k$  is the  $Q_\alpha$  value for the  $\alpha$ -decay channel connecting the states with excitation energies  $E_M$  and  $E_D$ , spin and parity  $J_M\pi_M$  and  $J_D\pi_D$  for the mother and daughter nuclei, respectively. The energies are in units of MeV.  $T_k$  is the partial half-life in seconds and  $\bar{\gamma}_k^2(r_l)$  is the equivalent reduced width in MeV for the decay channel. In the column “1-q.-p. states” the interpretation of the mother and daughter configurations as single quasiparticle states are listed. An odd proton(neutron) is indicated by  $\pi(\nu)$ . Fav, PC, SF, and OC indicate if the decay belongs in the group of (i) favored, (ii) parity change, (iii) spin flip, or (iv) orbital change decays, respectively.

Index	$Z$	$N$	$J_M\pi_M$	$E_M$	$J_D\pi_D$	$E_D$	$Q_k$	$T_k$	$\bar{\gamma}_k^2(r_l)$	1-q.-p. states	Group
1	61	84	5/2+	0	5/2+	0	2.322	$1.993 \times 10^{17}$	$1.463 \times 10^{-2}$	$\pi : d_{5/2} \rightarrow d_{5/2}$	Fav
2	62	85	7/2-	0	7/2-	0	2.311	$3.374 \times 10^{18}$	$8.318 \times 10^{-3}$	$\nu : f_{7/2} \rightarrow f_{7/2}$	Fav
3	63	84	5/2+	0	5/2+	0	2.991	$9.465 \times 10^{10}$	$1.889 \times 10^{-2}$	$\pi : d_{5/2} \rightarrow d_{5/2}$	Fav
4	65	84	11/2-	0.040	5/2+	0	4.117	$1.135 \times 10^6$	$6.043 \times 10^{-5}$	$\pi : h_{11/2} \rightarrow d_{5/2}$	PC
5	65	84	1/2+	0	5/2+	0	4.077	$8.877 \times 10^4$	$1.367 \times 10^{-3}$	$\pi : s_{1/2} \rightarrow d_{5/2}$	OC
6	65	84	1/2+	0	7/2+	0.330	3.748	$2.965 \times 10^8$	$6.439 \times 10^{-5}$	$\pi : s_{1/2} \rightarrow g_{7/2}$	SF
7	84	117	13/2+	0.424	13/2+	0.319	5.904	$1.841 \times 10^4$	$1.415 \times 10^{-3}$	$\nu : i_{13/2} \rightarrow i_{13/2}$	Fav
8	84	117	3/2-	0	5/2-	0.085	5.714	$2.869 \times 10^6$	$7.198 \times 10^{-5}$	$\nu : p_{3/2} \rightarrow f_{5/2}$	SF
9	84	117	3/2-	0	3/2-	0	5.799	$5.737 \times 10^4$	$1.405 \times 10^{-3}$	$\nu : p_{3/2} \rightarrow p_{3/2}$	Fav
10	84	119	5/2-	0	3/2-	0	5.496	$2.002 \times 10^8$	$1.172 \times 10^{-5}$	$\nu : f_{5/2} \rightarrow p_{3/2}$	SF
11	85	118	9/2-	0	9/2-	0	6.210	$1.644 \times 10^3$	$1.826 \times 10^{-3}$	$\pi : h_{9/2} \rightarrow h_{9/2}$	Fav
12	84	121	5/2-	0	5/2-	0	5.324	$1.565 \times 10^7$	$1.122 \times 10^{-3}$	$\nu : f_{5/2} \rightarrow f_{5/2}$	Fav
13	85	120	9/2-	0	9/2-	0	6.019	$1.614 \times 10^4$	$1.190 \times 10^{-3}$	$\pi : h_{9/2} \rightarrow h_{9/2}$	Fav
14	84	123	5/2-	0	5/2-	0	5.216	$9.943 \times 10^7$	$6.369 \times 10^{-4}$	$\nu : f_{5/2} \rightarrow f_{5/2}$	Fav
15	85	122	9/2-	0	9/2-	0	5.872	$7.535 \times 10^4$	$1.126 \times 10^{-3}$	$\pi : h_{9/2} \rightarrow h_{9/2}$	Fav
16	86	121	5/2-	0	3/2-	0.060	6.191	$3.993 \times 10^5$	$2.214 \times 10^{-5}$	$\nu : f_{5/2} \rightarrow p_{3/2}$	SF
17	86	121	5/2-	0	5/2-	0	6.251	$2.643 \times 10^3$	$1.830 \times 10^{-3}$	$\nu : f_{5/2} \rightarrow f_{5/2}$	Fav
18	87	120	9/2-	0	9/2-	0	6.900	$1.558 \times 10^1$	$2.098 \times 10^{-3}$	$\pi : h_{9/2} \rightarrow h_{9/2}$	Fav
19	83	126	9/2-	0	3/2+	0.204	2.933	$1.498 \times 10^{30}$	$4.518 \times 10^{-7}$	$\pi : h_{9/2} \rightarrow d_{3/2}$	PC
20	83	126	9/2-	0	1/2+	0	3.137	$5.997 \times 10^{26}$	$2.748 \times 10^{-6}$	$\pi : h_{9/2} \rightarrow s_{1/2}$	PC SF
21	84	125	1/2-	0	3/2-	0.263	4.716	$5.836 \times 10^{11}$	$1.081 \times 10^{-4}$	$\nu : p_{1/2} \rightarrow p_{3/2}$	SF
22	84	125	1/2-	0	1/2-	0.002	4.977	$4.071 \times 10^9$	$3.538 \times 10^{-4}$	$\nu : p_{1/2} \rightarrow p_{1/2}$	Fav
23	84	125	1/2-	0	5/2-	0	4.979	$1.632 \times 10^{10}$	$8.544 \times 10^{-5}$	$\nu : p_{1/2} \rightarrow f_{5/2}$	OC
24	85	124	9/2-	0	9/2-	0	5.757	$4.750 \times 10^5$	$5.820 \times 10^{-4}$	$\pi : h_{9/2} \rightarrow h_{9/2}$	Fav
25	86	123	5/2-	0	3/2-	0.155	6.001	$4.670 \times 10^6$	$1.255 \times 10^{-5}$	$\nu : f_{5/2} \rightarrow p_{3/2}$	SF
26	86	123	5/2-	0	1/2-	0.144	6.011	$7.200 \times 10^6$	$7.241 \times 10^{-6}$	$\nu : f_{5/2} \rightarrow p_{1/2}$	OC
27	86	123	5/2-	0	5/2-	0	6.156	$1.022 \times 10^4$	$1.138 \times 10^{-3}$	$\nu : f_{5/2} \rightarrow f_{5/2}$	Fav
28	87	122	9/2-	0	9/2-	0	6.777	$5.674 \times 10^1$	$1.550 \times 10^{-3}$	$\pi : h_{9/2} \rightarrow h_{9/2}$	Fav
29	84	127	9/2+	0	13/2+	1.633	5.961	$6.370 \times 10^4$	$1.442 \times 10^{-4}$	$\nu : g_{9/2} \rightarrow i_{13/2}$	OC
30	84	127	9/2+	0	3/2-	0.898	6.697	$9.609 \times 10^1$	$8.560 \times 10^{-5}$	$\nu : g_{9/2} \rightarrow p_{3/2}$	PC
31	84	127	9/2+	0	5/2-	0.570	7.025	$9.451 \times 10^1$	$5.584 \times 10^{-6}$	$\nu : g_{9/2} \rightarrow f_{5/2}$	PC SF
32	84	127	9/2+	0	1/2-	0	7.594	$5.217 \times 10^{-1}$	$1.366 \times 10^{-5}$	$\nu : g_{9/2} \rightarrow p_{1/2}$	PC SF
33	85	126	9/2-	0	7/2-	0.743	5.240	$2.497 \times 10^9$	$5.252 \times 10^{-5}$	$\pi : h_{9/2} \rightarrow f_{7/2}$	SF
34	85	126	9/2-	0	11/2-	0.670	5.313	$6.834 \times 10^8$	$7.503 \times 10^{-5}$	$\pi : h_{9/2} \rightarrow h_{11/2}$	SF, 2+
35	85	126	9/2-	0	9/2-	0	5.982	$6.213 \times 10^4$	$3.520 \times 10^{-4}$	$\pi : h_{9/2} \rightarrow h_{9/2}$	Fav
36	86	125	1/2-	0	9/2-	0.811	5.154	$3.285 \times 10^{10}$	$4.153 \times 10^{-5}$	$\nu : p_{1/2} \rightarrow h_{9/2}$	OC, 2+
37	86	125	1/2-	0	7/2-	0.586	5.379	$1.282 \times 10^9$	$5.621 \times 10^{-5}$	$\nu : p_{1/2} \rightarrow f_{7/2}$	SF
38	86	125	1/2-	0	3/2-	0.236	5.729	$7.103 \times 10^6$	$1.514 \times 10^{-4}$	$\nu : p_{1/2} \rightarrow p_{3/2}$	SF
39	86	125	1/2-	0	1/2-	0.069	5.897	$3.038 \times 10^5$	$5.407 \times 10^{-4}$	$\nu : p_{1/2} \rightarrow p_{1/2}$	Fav
40	86	125	1/2-	0	5/2-	0	5.965	$5.591 \times 10^5$	$1.399 \times 10^{-4}$	$\nu : p_{1/2} \rightarrow f_{5/2}$	OC
41	87	124	9/2-	0	13/2-	0.687	5.976	$2.325 \times 10^6$	$8.957 \times 10^{-5}$	$\pi : h_{9/2} \rightarrow j_{13/2}$	OC, 2+
42	87	124	9/2-	0	11/2-	0.644	6.019	$3.720 \times 10^6$	$3.528 \times 10^{-5}$	$\pi : h_{9/2} \rightarrow h_{11/2}$	SF, 2+
43	87	124	9/2-	0	7/2-	0.344	6.319	$5.167 \times 10^5$	$1.157 \times 10^{-5}$	$\pi : h_{9/2} \rightarrow f_{7/2}$	SF
44	87	124	9/2-	0	9/2-	0	6.663	$2.138 \times 10^2$	$1.053 \times 10^{-3}$	$\pi : h_{9/2} \rightarrow h_{9/2}$	Fav
45	84	129	9/2+	0	11/2+	0.779	7.758	$8.750 \times 10^{-2}$	$2.397 \times 10^{-5}$	$\nu : g_{9/2} \rightarrow i_{11/2}$	SF
46	84	129	9/2+	0	9/2+	0	8.537	$4.200 \times 10^{-6}$	$3.619 \times 10^{-3}$	$\nu : g_{9/2} \rightarrow g_{9/2}$	Fav
47	85	128	9/2-	0	9/2-	0	9.254	$1.250 \times 10^{-7}$	$5.171 \times 10^{-3}$	$\pi : h_{9/2} \rightarrow h_{9/2}$	Fav
48	87	126	9/2-	0	9/2-	0	6.905	$3.479 \times 10^1$	$6.965 \times 10^{-4}$	$\pi : h_{9/2} \rightarrow h_{9/2}$	Fav
49	88	125	1/2-	0	5/2-	0	6.860	$4.567 \times 10^2$	$2.102 \times 10^{-4}$	$\nu : p_{1/2} \rightarrow f_{5/2}$	OC

deformation parameter  $|\beta_2| < 0.1$  [27]. Only decays starting and ending in states where the spin  $j_{\text{exp}}$  and parity  $\pi_{\text{exp}}$  are assigned in the ENSDF database [28] are considered. States where spin and parity assignments are weak are excluded.

The adopted SHFB approach can only describe one-quasiparticle states, Eqs. (1) and (2). To exclude more complicated states, only the lowest-energy state of a given spin  $j_{\text{exp}}$  and parity  $\pi_{\text{exp}}$  is considered. This gives the

49 different  $\alpha$  decays shown in Table II. Based on the spin and parity assignments, each state is assigned the lowest-energy quasiparticle  $\beta_{1ljm}^\dagger$ , Eq. (B1), with orbital angular momentum  $l$  and total spin  $j$  so that the parity  $\pi$  and spin match the corresponding experimental values,

$$\pi = \pi_{\text{exp}}, \quad j = j_{\text{exp}}. \quad (22)$$

### C. Hindrance factors and selection rules

$\alpha$  decay of an odd nucleus is generally slower than the  $\alpha$  decay of even-even neighbors. To quantify this one can introduce a hindrance factor (HF). It is defined as the ratio of the partial half-life  $T_k$  for an  $\alpha$ -decay channel of an odd nucleus, to a reference half-life  $T_{\text{ref}}$  obtained from a one-body model for  $\alpha$  decay fitted to gs-gs decays of even-even nuclei (i.e.,  $L_\alpha = 0$ ),

$$\text{HF}_k = \frac{T_k}{T_{\text{ref}}(N, Z, Q_{\alpha k}^{\text{exp}})}. \quad (23)$$

The HF thus accounts for structural changes from the odd particle and the centrifugal barriers for the different allowed  $L_\alpha$ . From experimentally deduced HF-values different amounts of hindrance have been associated with different classes of decay scenarios [7]: The smallest HF  $\sim 1$ –4 corresponds to a favored transition, where the odd nucleon stays in the same orbital. A HF  $\sim 100$ –1000 indicates a change in parity of the mother nucleus state and the state of the daughter,  $\pi_M/\pi_D = -1$ , but with the spin projections of mother and daughter states being parallel  $\Delta s = 0$ . A HF  $> 1000$  indicates both a change in parity and in spin projection,  $\pi_M/\pi_D = -1$  and  $|\Delta s| = 1$ .

It is one aim of the current work to investigate to what extent these selection rules can be applied to near-spherical odd- $A$   $\alpha$  emitters, and especially if the observed variation of the hindrance can be reproduced in the microscopic calculations. We consider the following four groups:

- (i) *Favored*. Similar odd quasiparticle states in mother and daughter,  $k_M = k_D, l_M = l_D, I_M = I_D$ .
- (ii) *Spin flip*. Different spin projections  $|\Delta s| = 1$ , i.e.,  $I_M = l_M \pm \frac{1}{2}, I_D = l_D \mp \frac{1}{2}$ .
- (iii) *Parity change*.  $\pi_M/\pi_D = -1$ , i.e., different parity  $(-1)^{l_M} = (-1)^{l_D+1}$ .
- (iv) *Orbital change*. Different quasiparticle states, but same spin projection and parity, i.e.,  $\Delta s = 0$  and  $\pi_M/\pi_D = 1$ .

With this classification some decays belong to both groups (ii) and (iii).

To compare with microscopic results, Eq. (23) can be rewritten,

$$\text{HF}_k = \frac{\gamma_{\text{ref}}^2(r_t)}{\bar{\gamma}_k^2(r_t)}, \quad (24)$$

where Eq. (20) was used, and where the reference reduced width  $\gamma_{\text{ref}}^2(r_t)$  is related to  $T_{\text{ref}}$  through,

$$T_{\text{ref}}(N, Z, Q_{\alpha k}^{\text{exp}}) = \frac{\hbar \ln(2)}{2P_0(Q_{\alpha k}^{\text{exp}}, r_t) \gamma_{\text{ref}}^2(r_t)}. \quad (25)$$

The penetrability  $P_0$  describes the  $s$ -wave tunneling of a preformed  $\alpha$  particle. In a simple one-body model one effectively fits the reduced width  $\gamma_{\text{ref}}^2(r_t)$  to data. An equivalent measure of the hindrance is thus to compare the reduced width  $\bar{\gamma}_k^2(r_t)$  to an average reduced width  $\langle \gamma_0^2(r_t) \rangle$  for even-even nuclei. In this work we use the geometric mean reduced width obtained from experimental data for the gs-gs  $\alpha$  decays of the 48 near-spherical even nuclei studied in the previous work [15],  $\gamma_{\text{ref}}^2(r_t) = 4.10$  keV.

## IV. RESULTS FOR KNOWN $\alpha$ DECAYS

### A. Decay widths

The ratios of the calculated decay widths to the corresponding experimental values for the 49 cases in Table II are shown in Fig. 1. The different panels show results obtained with different density dependence of the effective pairing interaction. The theoretical decay widths for most cases are within a factor of 3 from the experimental values, shown by the dotted lines. For some cases the calculated decay widths are much smaller than the experimental value. For the four cases 34, 36, 41, and 42, marked with “2+” in the figure, the state of the daughter nucleus is interpreted as being dominated by the odd particle coupled to a  $2^+$  configuration of the even-numbered particle species [28]. The four daughter states are the  $11/2^-$  state in  $^{207}_{83}\text{Bi}_{124}$  (case 34), the  $9/2^-$  state in  $^{207}_{84}\text{Po}_{123}$  (case 36), and the  $13/2^-$  and  $11/2^-$  states in  $^{207}_{85}\text{At}_{122}$  (cases 41 and 42, respectively). These situations are outside the domain of the current model, where we assume one-quasiparticle states for the mother and daughter nucleus. In the following we shall exclude these four cases. The remaining cases in Table II are denoted data set I.

The decay width for three other cases,  $^{211}_{85}\text{At}_{126}$  (case 33),  $^{211}_{87}\text{Fr}_{124}$  (case 43), and  $^{213}_{84}\text{Po}_{129}$  (case 45), also come out too small in the calculations. Here the model should be applicable, and the discrepancy deserves further investigation. A common property of these three cases is that the odd particle in the daughter nucleus has an unusually small occupation in the mother nucleus. The occupation probability is defined,

$$n_{klj}^M = \sum_{k'} V_{k'k}^{(M)lj} V_{k'k}^{(M)lj*}, \quad (26)$$

where  $V^{(M)}$  is the HFB  $V$  matrix for the mother nucleus; cf. Eq. (B1). For these three cases  $n_{1l_D j_D}^M \approx 0.05$ , while for all other cases this occupation is larger,  $n_{1l_D j_D}^M > 0.1$ . How these small occupations influence the decay width is discussed in Sec. V.

The root-mean-square logarithmic deviation from experiment is defined,

$$\text{RMS} = \sqrt{\frac{1}{n} \sum_{i=1}^n (\log_{10}[\Gamma_{(i)}^{\text{th}}/\Gamma_{(i)}^{\text{exp}}])^2}. \quad (27)$$

A factor of 10 deviation thus gives RMS = 1, while a perfect agreement gives RMS = 0. For data set I the deviation is RMS = {0.68, 0.72, 0.79} for SLy4 with volume, mixed, and surface pairing, respectively. If the three cases with unusual small occupations  $n_{1l_D j_D}^M$  (cases 33, 43, and 45) are

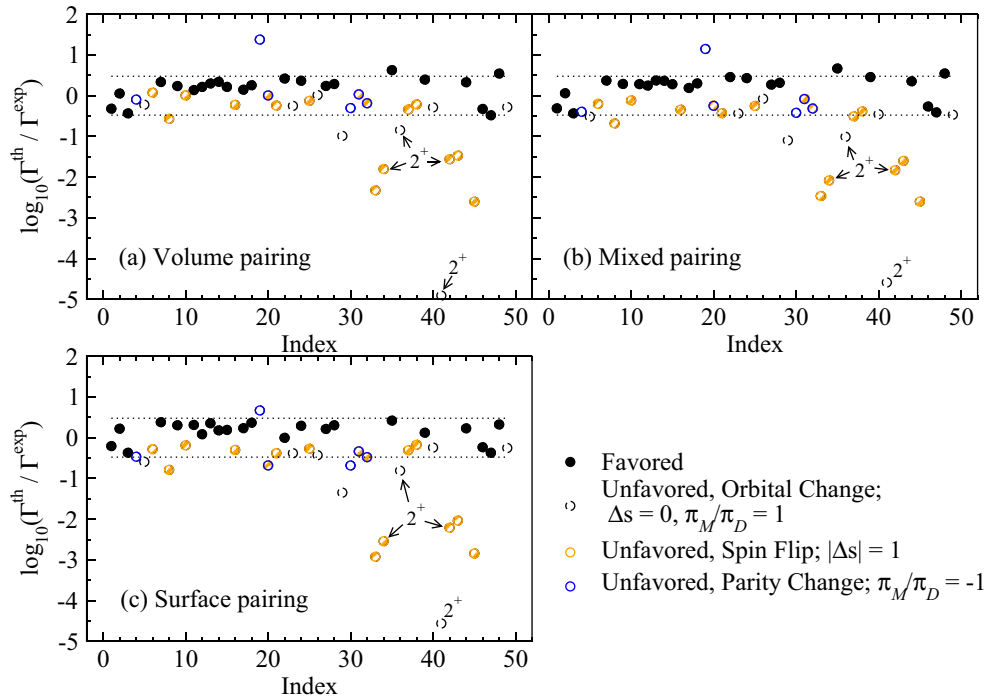


FIG. 1. (Color online) Logarithm of the ratio of the theoretical decay width  $\Gamma_{th}$  to the experimental value  $\Gamma_{exp}$  for the  $\alpha$ -decaying odd- $A$  nuclei in Table II. The Skyrme interaction SLy4 combined with volume (a), mixed (b), or surface pairing (c) is used in the calculations. The dotted lines indicate a deviation from experiment by a factor of 3.

excluded, the RMS improves to  $RMS = \{0.39, 0.44, 0.42\}$ . This corresponds to a deviation less than a factor of 3 from the experimental values for odd- $A$  nuclei, shown by the dotted lines in Fig. 1.

### B. Reduced widths and hindrance factors

Figure 2 shows the reduced widths for  $\alpha$  decay of odd- $A$  nuclei in data set I. For comparison reduced widths for the 48 ground-state-to-ground-state decays of near-spherical even-even nuclei studied in the previous article [15], are also

shown. In Fig. 2(a) the widths are obtained from experimental data, Eq. (21), while Fig. 2(b) shows the microscopic results, Eq. (20), obtained with surface pairing. The experimental reduced widths for favored odd decays follow closely the trend of the even-even decays. The theoretical results reproduce the variation with neutron number in both the even and odd favored decays reasonably well. For the favored odd case the main component of the formation amplitude corresponds to the odd quasiparticle acting as a spectator to the formation of the  $\alpha$  particle from the HFB vacuum, which explains the similarity to the even-even reduced widths.

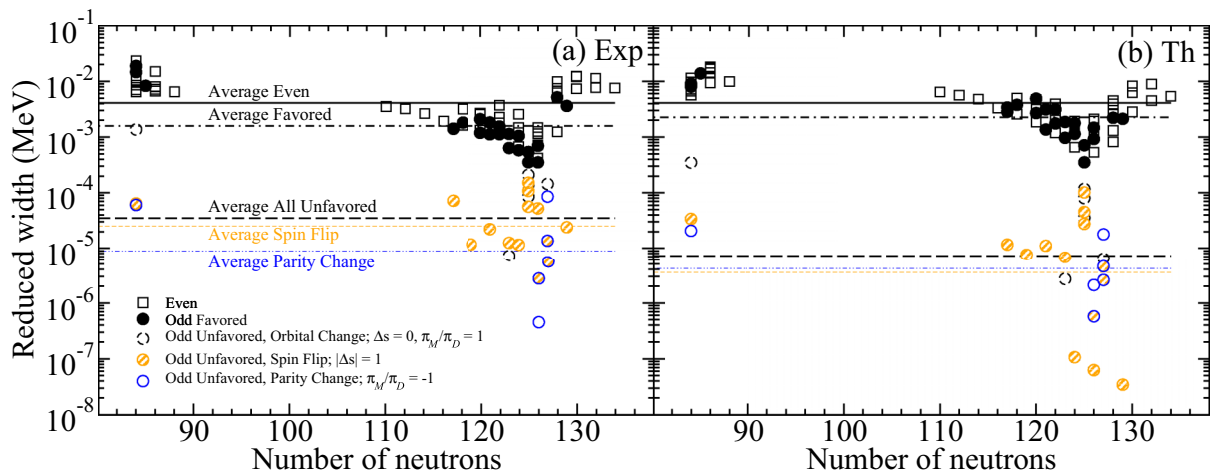


FIG. 2. (Color online) Reduced widths for data set I. (a) The experimental reduced width [Eq. (21)]. (b) The microscopic reduced width [Eq. (20)] obtained with SLy4 and surface pairing.

TABLE III. Geometric mean hindrance factors  $M_{\text{HF}}$  for different groups of  $\alpha$  decays. No. is the number of data points in the group. Expt. refers to values extracted from the experimental data, Vol., Mix., and Surf. refer to results from the microscopic calculations with SLy4 and volume, mixed, and surface pairing, respectively.

Group	No.	$M_{\text{HF}}$			
		Expt.	Vol.	Mix.	Surf.
Even-even	48	1	1	1	1
Favored odd	22	2.57	1.71	1.51	1.81
Spin flip	14	163	625	854	1165
Parity change	6	462	335	508	983
Orbital change	6	33.2	71.7	105	115
All unfavored odd	23	117	294	417	562

The unfavored decays have smaller reduced widths than the favored decays, and are generally well reproduced in the calculations. The hindrance factor, Eq. (24), is defined with the reference reduced width chosen as the geometric mean reduced width for the even-even decays shown in Fig. 2. This mean value is shown by a full horizontal line in the figure. The other lines in the figure show the geometric mean reduced width for different groups of decays of odd nuclei. The distance between the average for the even-even nuclei to those of the odd nuclei corresponds to the geometric mean hindrance factor  $M_{\text{HF}}$ ,

$$\log_{10}(M_{\text{HF}}) = \frac{1}{n} \sum_{k=1}^n \log_{10}(\text{HF}_k). \quad (28)$$

The mean hindrance factors  $M_{\text{HF}}$  and corresponding standard deviations  $\sigma_{\text{HF}}$  obtained from the experimental data and in the calculations are summarized in Tables III and IV.

The hindrance factors are classified in the four groups defined in Sec. III C. In the experimental data, the favored odd decays are on average hindered by a factor 2.6, and when there is a change in parity by a factor 462. This agrees with the empirical rules of Ref. [7]. When the decay is characterized as a spin flip, the geometrical mean hindrance in the data is a factor 163. Finally, orbital change gives a mean hindrance factor of 33. In the data set there are three cases where there is both a change in parity and a spin flip,  $^{209}\text{Bi}_{126}$  (case 20),  $^{211}\text{Po}_{127}$  (cases 31 and 32) with corresponding hindrance factors 1490, 735, and 300, respectively. The values for Po are smaller than expected from the empirical rule of Ref. [7].

TABLE IV. Similar to Table III, but showing the corresponding standard deviations  $\sigma_{\text{HF}}$ .

Group	No.	$\sigma_{\text{HF}}$			
		Expt.	Vol.	Mix.	Surf.
Even-even	48	2.74	1.91	1.82	2.47
Favored odd	22	2.97	1.78	1.73	2.36
Spin flip	14	3.22	9.13	8.39	12.7
Parity change	6	7.19	3.06	3.07	3.91
Orbital change	6	5.42	5.18	4.41	6.28
All unfavored odd	23	5.44	8.42	7.65	11.1

The reduced widths of spin-flip and parity-change decays shown in Fig. 2, show a quite large variation around the respective mean values. This is reflected in the geometrical standard deviations in Table IV, where  $\sigma_{\text{HF}} = 1$  corresponds to no variation and  $\sigma_{\text{HF}} = 10$  to a factor 10 larger or smaller hindrance factor than the geometrical mean. The hindrance factors for unfavored decays in a given group can vary by an order of magnitude when comparing nearby nuclei. This implies that the simple empirical rule can only be used as a rough indication of the hindrance. Considering the large fluctuations in reduced widths, one cannot deduce the hindrance of an unfavored decay channel based on which subgroup of decays it belongs to. For simple estimates, it is more useful to consider only two groups, favored and unfavored decays.

The hindrance obtained in the microscopic calculations agrees well with the hindrance seen in the experimental data, except for the spin-flip category, where the mean hindrance is increased by the large errors in the calculated reduced widths for the cases 33, 43, and 45, discussed in the previous subsection. If these cases are ignored a better agreement to data is obtained. For example, using surface pairing we get for the spin-flip group  $M_{\text{HF}} = 386$  and  $\sigma_{\text{HF}} = 4.26$  that are closer to the experimental numbers  $M_{\text{HF}} = 161$  and  $\sigma_{\text{HF}} = 3.63$ .

## V. ROLE OF PAIRING

Pairing correlations play a most important role for the formation of the  $\alpha$  particle in the mother nucleus. The sensitivity of the calculated decay widths for odd- $A$  nuclei to the strength and density dependence of the pairing force is investigated in Sec. V A. An approximate relation for the formation amplitude, where the effect of the pairing can be separated out, is presented in Sec. V B, and used to analyze the variation of the reduced widths in Sec. V C. Section V D contains a discussion on the three decays widths (cases 33, 43, and 45) which come out too small in the results presented in Sec. IV.

### A. Sensitivity to pairing force properties

To investigate the sensitivity of the formation amplitude in the odd case, we consider the reduced set of decays  $I'$ , corresponding to data set I but excluding the three cases where the calculations give unusually small occupations, 33, 43 and 45.

The dependence on the pairing strength is shown in Fig. 3. It shows the mean value of  $\log_{10}(\Gamma^{\text{th}}/\Gamma^{\text{exp}}) = \log_{10}[\bar{\gamma}_{\text{th}}^2(r_t)/\bar{\gamma}_{\text{exp}}^2(r_t)]$  for the favored decays (F), and unfavored decays (U) as a function of a scaling of the pairing interaction strength. 1.0 corresponds to the pairing interaction giving realistic odd-even staggering, and 0.5 and 1.5 to decreasing or increasing the interaction strength by 50%. The phenomenological scaling factor  $\mathcal{S}$  [Eq. (18)] is held constant for all pairing strengths.

The formation amplitude of the unfavored decays is less sensitive to the strength of the pairing, as seen by the steeper slope of the mean value for the favored decays (solid symbols) than for the unfavored (open symbols) in Fig. 3. This behavior is because for unfavored decay, the part of the  $\alpha$  particle belonging to the odd-numbered particle species is

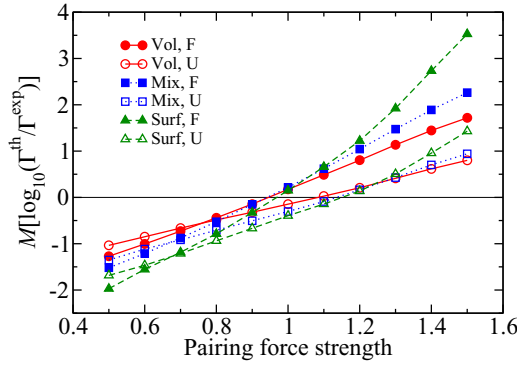


FIG. 3. (Color online) Mean value of  $\log_{10}(\Gamma^{\text{th}}/\Gamma^{\text{exp}})$  for Data set I. The circles, squares, and triangles show results for SLy4 + volume, mixed, and surface pairing, respectively. Solid symbols indicate favored decays, while open symbols indicate unfavored decays.

not formed from time-reversed pairs of nucleons. This is seen most clearly in the approximate relations in Sec. V B. Because of the different dependencies of the favored and hindered decays, the overall hindrance is sensitive to the value of the pairing strength. At the realistic strength 1.0 the mean ratio to experiment for the favored decays is around a factor 1.4, while for the unfavored decays around a factor 0.5. From Fig. 3, we see that the mean agreement with experiment for the two groups would coincide when using a reduced pairing strength, roughly a factor  $\sim 0.7$  of the realistic value. The different behavior of the favored and hindered groups suggests that a more realistic treatment of the blocking effect on the pairing might improve the overall description of the data. Blocking would approximately correspond to a reduction of the pairing strength and would move the mean values of the favored and hindered groups closer to each other.

The corresponding standard deviations are shown in Fig. 4. The standard deviations  $\sigma$  for the unfavored decays are generally more sensitive to the pairing strength than for the favored decays. The smallest  $\sigma$  for the hindered cases is obtained when keeping the pairing strength close to the realistic value. For the case of even-even nuclei the smallest deviation from experiment is obtained when using the surface pairing [15], cf. Table I. Figure 4 shows that surface pairing

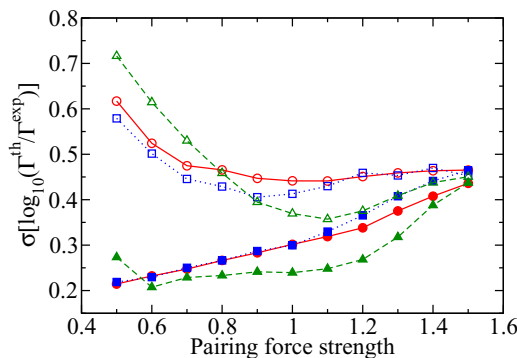


FIG. 4. (Color online) Similar to Fig. 3, but showing instead the standard deviation of  $\log_{10}(\Gamma^{\text{th}}/\Gamma^{\text{exp}})$ .

also gives a slightly better description than volume and mixed pairing when considering unfavored and favored groups of odd-nucleus  $\alpha$  decays separately.

### B. Approximate pairing dependence of the formation amplitude

To better understand the variation in the reduced width from pairing, we consider some simplifying approximations for the formation amplitude. The expressions for the transfer amplitudes Eqs. (B5) and (B8) entering in the formation amplitude become simpler if one considers a BCS description of the mother and daughter nuclei; see Eqs. (B12)–(B14) in Appendix B.

By making the approximation that the mother and daughter vacua are the same,  $|M_{00}\rangle \approx |D_{00}\rangle$ , and replacing the overlaps of four-particle configurations with the  $\alpha$ -particle wave function with an average value, one obtains an approximate relation for the pairing dependence of the formation amplitude [11],

$$g_0^F(R'_\alpha) \sim \Delta N_\pi \Delta N_\nu g_0^{\text{average}}(R'_\alpha), \quad (29)$$

where  $\Delta N_{\pi(\nu)}$  is the standard deviation of the number of protons (neutrons) in the BCS wave function.

For the second term in Eq. (13), which is the only active term in the case of an unfavored decay, the sum over two-particle configurations for the odd-numbered species is restricted to a single configuration by Eq. (B14). This implies that there will be no pairing enhancement of the formation amplitude for the odd-numbered species. In Ref. [11] the reduction in amplitude for the hindered decay channels was seen to come both from this fact, and that the overlap of the two different orbitals of the odd particles with the  $\alpha$  particle are generally smaller than for two time-reversed conjugate orbitals.

If one makes a further approximation that the formation amplitude is separable in a proton and a neutron part, the approximate pairing dependence for an odd number of protons becomes

$$g_{L_\alpha}^H(R'_\alpha) \sim p h_{L_\alpha}(R'_\alpha), \quad (30)$$

where the pairing factor  $p$  is given by

$$p = \frac{u_{k_M l_M j_M}^{D\pi} v_{k_D l_D j_D}^{M\pi}}{\sqrt{2j_M + 1}} \Delta N_\nu, \quad (31)$$

with the BCS amplitudes  $u_{k_M l_M j_M}^{D\pi}$  and  $v_{k_D l_D j_D}^{M\pi}$  defined in Appendix B. For the HFB case we consider the pairing factor,

$$p = \sqrt{\frac{(1 - n_{k_M l_M j_M}^{D\pi}) n_{k_D l_D j_D}^{M\pi}}{2j_M + 1}} \Delta N_\nu, \quad (32)$$

where  $n_{klj}^{D(M)}$  is the occupation probability, Eq. (26), for the daughter (mother). The factor  $h_{L_\alpha}(R'_\alpha)$  depends on the overlap of the single-particle wave functions of the odd particles in the mother and daughter nucleus with the  $\alpha$  particle. The reduced width can thus be estimated as  $\gamma^2 \sim p^2$ .

### C. Variation of reduced widths

The upper panel of Fig. 5 shows the reduced widths, Eq. (20), for  ${}_{84}\text{Po}_{117}$  (case 8), where the odd particle occupies

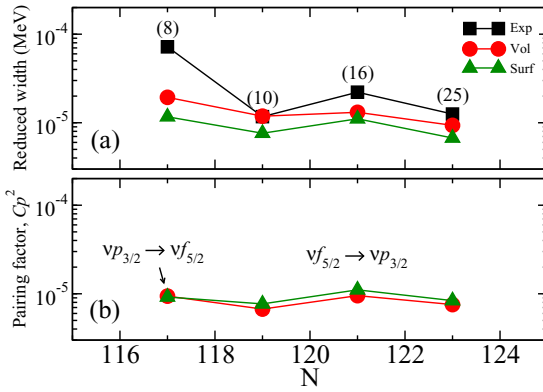


FIG. 5. (Color online) (a) Reduced widths for cases (8), (10), (16), and (25) in Table II. (b) The corresponding pairing factors  $p^2$  multiplied by a constant  $C$ . The constant is chosen to set  $Cp^2$  equal to the theoretical reduced width of  $^{86}\text{Rn}_{121}$  when surface pairing is employed, giving  $C = 3.82 \times 10^{-5}$  MeV.

the orbital  $\nu p_{3/2}$  in the mother nucleus and  $\nu f_{5/2}$  in the daughter, and for decays of  $^{84}\text{Po}_{119}$  (case 10),  $^{86}\text{Rn}_{121}$  (case 16), and  $^{84}\text{Rn}_{123}$  (case 25) where the odd particle orbital changes from  $\nu f_{5/2} \rightarrow \nu p_{3/2}$ . In the lower panel the corresponding pairing factors squared  $p^2$ , Eq. (32), appearing in the approximate relation (30), are shown. There is a correlation in the variation with neutron number of these two quantities: When the orbitals occupied by the odd particle are the same in different hindered decays, the fluctuation in the reduced width can be qualitatively explained by the variation of these simple pairing properties. A similar comparison can be made for decays where the odd-particle orbitals involved are different. In that case there is less correlation between the two quantities, because of the difference in the wave functions for the odd particle orbitals entering in the overlap with the  $\alpha$  particle.

#### D. Decay widths not reproduced in the calculations

Equation (32) provides a simple picture describing unfavored  $\alpha$  decay, i.e., when the odd nucleon changes orbital. To get a large reduced width, the orbital  $k_D$  of the odd nucleon in the daughter nucleus should be fully occupied in the mother-nucleus vacuum,  $n_{k_D^{M\pi}}^{M\pi} = 1$ , while the orbital  $k_M$  of the odd nucleon in the mother nucleus should be empty in the daughter-nucleus vacuum,  $n_{k_M^{D\pi}}^{D\pi} = 0$ . The  $\alpha$  particle is thus formed by taking one of the nucleons from the orbital  $k_D$ , leaving the odd nucleon of the daughter nucleus, and taking the other nucleon from the initial odd-nucleon orbital in the mother nucleus  $k_M$ . For unfavored decay leading to a daughter nucleus where the odd quasiparticle corresponds to creating a hole in the daughter-nucleus vacuum, the occupation probability of this orbital in the mother-nucleus vacuum  $n_{k_D^{M\pi}}^{M\pi}$  is close to 1. For cases where the odd nucleon in the daughter nucleus occupies a high lying particle state  $n_{k_D^{M\pi}}^{M\pi}$  can be small. The three cases (33, 43, and 45) where the decay width comes out too small in the calculations corresponds to this situation.

Figure 6 shows single-particle energies for  $^{208}\text{Pb}_{126}$ , close to the  $\alpha$ -decaying nuclei in question. In the unfavored  $\alpha$  decays of  $^{211}_{85}\text{At}_{126}$  (case 33) and  $^{211}_{87}\text{Fr}_{124}$  (case 43) the odd proton

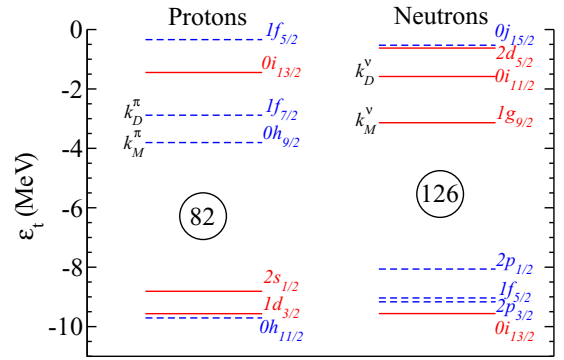


FIG. 6. (Color online) Single-particle energies  $\epsilon_t$  for  $^{208}\text{Pb}_{126}$  obtained with SLy4.  $k_M^{\pi(v)}$  denotes the orbital of the odd particle in the mother nucleus and  $k_D^{\pi(v)}$  in the daughter nucleus for the unfavored odd proton(neutron) decays discussed in the text.

quasiparticle in the mother nucleus  $k_M^\pi$  is in the  $0h_{9/2}$  shell, above the  $Z = 82$  gap. In the daughter nucleus the odd-proton quasiparticle  $k_D^\pi$  is in the  $1f_{7/2}$  shell, above  $0h_{9/2}$ . For the decay of  $^{213}_{84}\text{Po}_{129}$  (case 45), the odd neutron quasiparticle changes from  $k_M^v = 1g_{9/2}$  in the mother nucleus to  $k_D^v = 0i_{11/2}$  in the daughter nucleus. The spherical Hartree-Fock (HF) single-particle level  $0i_{11/2}$  is  $\sim 1.5$  MeV above  $1g_{9/2}$ , and both levels sit above the  $N = 126$  gap. These three cases stand out with small occupations  $n_{k_D^{M\pi}}^{M\pi} < 0.1$ , small pairing factors  $p^2 < 0.05$ , and too small decay widths compared to experiment. The poor description of the three cases is not significantly improved when the pairing interaction strength is changed as in Sec. V A.

The HF single-particle energies around the  $Z = 82$  and  $N = 126$  gaps obtained with SLy4 for  $^{208}\text{Po}_{126}$  agree within 1 MeV with experimental spectra [19]. The difference of the quasiparticle energy with the lowest quasiparticle energy gives an approximate excitation energy of the daughter state. These energies agree within 0.6 MeV with experimental data for the three cases. The reasonable description of the single-particle energies and that the three cases stand out for a range of pairing strengths point to the need to improve the treatment of pairing correlations. An increase of the occupation probability of orbitals above the gaps should lead to a larger formation amplitude for these cases, giving better agreement with experiment.

## VI. PREDICTIONS FOR $\alpha$ DECAY OF ODD SUPERHEAVY NUCLEI

In this section we present results for the gs-gs partial  $\alpha$ -decay half-lives  $T_{\text{gs-gs}}$  of even-even and odd- $A$  superheavy nuclei. A complete description of the  $\alpha$ -decay properties requires a description of both the low-lying states and the  $Q_\alpha$  values. To fully describe the  $\alpha$ -decay spectra of superheavy nuclei thus requires accurate spectroscopic predictions, which are not available from current models applicable to the heaviest elements. Here we instead focus on the  $T_{\text{gs-gs}}$ , which gives an upper limit of the total half-life, and indicates where one might observe  $\alpha$  decay to excited states.

The Skyrme force SLy4 combined with the mixed pairing is used. The volume and surface pairing give slightly smaller RMS for the known  $\alpha$  decays of near-spherical odd- $A$  nuclei; see Sec. IV A. On the other hand, fits of known masses suggest that a surface pairing is less realistic [29], while the volume pairing gives the poorest description of even-even  $\alpha$  decays. To demonstrate the accuracy of the method when the  $Q_\alpha$  values and the level structure of the nuclei are known we first show results for Po isotopes, in Sec. VI A. Predictions for superheavy nuclei, using calculated  $Q_\alpha$  values and ground-state configurations, are then presented in Sec. VI B.

When  $\alpha$  decay to the ground state is hindered one can observe decays populating excited states. The observation of subsequent electromagnetic decay of these states can then be used to obtain spectroscopic information of the superheavy elements. Which state is populated depends on the balance of the hindrance of the more energetic gs-gs decay and the smaller  $Q_\alpha$  value leading to the excited state. The competition between unfavored gs-gs and favored gs-es  $\alpha$  decay is discussed and investigated in detail for a few cases in Sec. VI C. Finally, Sec. VI D contains a discussion on the ordering of single-particle states in different models, affecting which gs-gs decays are hindered. The sensitivity of the  $Q_\alpha$  values and half-lives to neglected beyond mean-field effects is briefly discussed.

### A. Ground-state $\alpha$ -decay half-lives for Po isotopes

The ground-state  $\alpha$ -decay properties of odd Po isotopes are displayed in Table V, with experimental data from [28]. The one-quasiparticle description of the ground state is selected in the same way as in Sec. III B, except that we also consider decays where the spin and parity assignments in [28] are weaker. For Po and Pb isotopes with  $N \leq 113$  the assignments are based on systematics. The present model is applicable only for near-spherical nuclei. However, to get

TABLE V. Ground-state-to-ground-state  $\alpha$ -decay properties of odd Po isotopes. Experimental  $Q_{\text{gs-gs}}^{\text{exp}}$  values in MeV, and gs-gs half-lives  $T_{\text{gs-gs}}^{\text{exp}}$  in seconds from [28].  $\beta_{M(D)}$  denotes the theoretical quadrupole deformation of the mother(daughter) nucleus [27].

$N$	$Q_{\text{gs-gs}}^{\text{exp}}$	$T_{\text{gs-gs}}^{\text{exp}}$	l-q.-p. states	$\beta_M$	$\beta_D$
103	7.979	$1.400 \times 10^{-3}$	$p_{3/2} \rightarrow p_{3/2}$	0.311	0.009
105	7.701	$4.375 \times 10^{-2}$	$p_{3/2} \rightarrow p_{3/2}$	0.274	0.009
107	7.501	$1.477 \times 10^{-1}$	$p_{3/2} \rightarrow i_{13/2}$	0.275	0.000
109	7.093	$3.737 \times 10^{-1}$	$p_{3/2} \rightarrow p_{3/2}$	-0.215	0.000
111	6.746	$6.187 \times 10^0$	$p_{3/2} \rightarrow p_{3/2}$	0.071	0.000
113	6.412	$1.218 \times 10^2$	$p_{3/2} \rightarrow p_{3/2}$	0.062	0.000
115	6.074	$2.735 \times 10^3$	$p_{3/2} \rightarrow p_{3/2}$	0.000	0.009
117	5.799	$5.737 \times 10^4$	$p_{3/2} \rightarrow p_{3/2}$	0.000	0.000
119	5.496	$2.002 \times 10^8$	$f_{5/2} \rightarrow p_{3/2}$	0.000	0.000
121	5.324	$1.565 \times 10^7$	$f_{5/2} \rightarrow f_{5/2}$	0.018	0.000
123	5.216	$9.943 \times 10^7$	$f_{5/2} \rightarrow f_{5/2}$	-0.026	0.008
125	4.979	$1.632 \times 10^{10}$	$p_{1/2} \rightarrow f_{5/2}$	-0.008	-0.018
127	7.595	$5.217 \times 10^{-1}$	$g_{9/2} \rightarrow p_{1/2}$	-0.008	-0.008
129	8.537	$4.200 \times 10^{-6}$	$g_{9/2} \rightarrow g_{9/2}$	-0.008	-0.008
131	7.526	$1.781 \times 10^{-3}$	$g_{9/2} \rightarrow g_{9/2}$	0.020	0.008
133	6.662	$1.611 \times 10^0$	$g_{9/2} \rightarrow g_{9/2}$	0.031	0.009

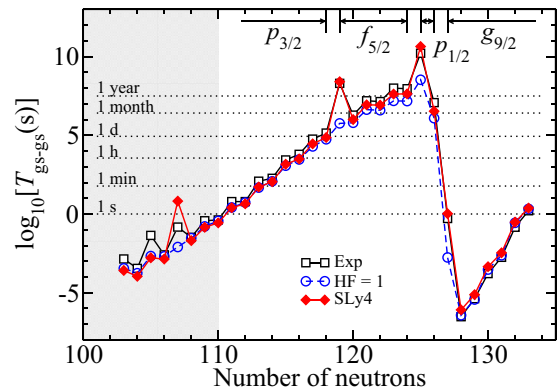


FIG. 7. (Color online) Ground-state-to-ground-state half-lives for Po isotopes. The experimental data are shown by the squares, results from the microscopic calculations by the diamonds, and half-lives giving a hindrance factor  $\text{HF} = 1$  by the circles. The shaded area shows where the mother nuclei are deformed,  $|\beta_M| > 0.1$ .

rough systematic estimates, deformed cases are occasionally considered. When the ground state is deformed the spherical  $j$  shell corresponding to the proposed Nilsson quantum numbers is used. The  $j$  shell is selected by tracing the deformed level to its spherical origin.

The gs-gs partial  $\alpha$ -decay half-lives are shown in Fig. 7. The diamonds show the theoretical half-lives obtained with SLy4 and mixed pairing. The experimental  $Q_{\text{gs-gs}}^{\text{exp}}$  values are used in the calculation. For the near-spherical Po isotopes, with  $N > 110$ , the model describes the experimental data well. The lighter,  $N < 110$ , Po isotopes have deformed ground states,  $|\beta_M| > 0.1$ , according to the theoretical mass table in Ref. [27], and the calculations are very approximative.

The circles show the reference half-lives  $T_{\text{ref}}$  (25), corresponding to a hindrance factor  $\text{HF} = 1$  in the definition (24). For the considered Po isotopes the half-lives vary over more than 17 orders of magnitude, mainly caused by the variations in the  $Q_\alpha$  values. The maximum in  $T$  corresponds to a minimum in  $Q_\alpha$  related to the  $N = 126$  shell closure. The distance in the figure between the partial half-life and the corresponding  $T_{\text{ref}}$  gives the hindrance factor, and shows the influence of differing structures of mother and daughter states.

The spherical  $j$  shell of the odd neutron in the mother nucleus is marked by the spectroscopic labels in the figure. The gs-gs  $\alpha$  decays of  $^{211}_{84}\text{Po}_{127}$ ,  $^{209}_{84}\text{Po}_{125}$ ,  $^{203}_{84}\text{Po}_{119}$  are unfavored because of a change of the  $j$  shell for the odd neutron, from  $j$  shells  $g_{9/2}$ ,  $p_{1/2}$ , and  $f_{5/2}$ ; see Table V and Fig. 6. These unfavored decays have a longer  $T_{\text{gs-gs}}$  compared to  $T_{\text{ref}}$ . The hindrance is well described in the microscopic calculations, as seen by the close agreement with experimental data.

### B. Ground-state $\alpha$ -decay half-lives for superheavy isotopes

The gs-gs  $\alpha$ -decay properties of odd- $A$  and even-even superheavy isotopes with  $107 \leq Z \leq 120$ ,  $172 \leq N \leq 187$  are studied. To obtain the ground-state configurations and  $Q_{\text{gs-gs}}$  values, axially symmetric SHFB calculations are performed using the code HFBTHO [20]. The same SLy4 Skyrme force and mixed pairing as used in the microscopic  $\alpha$ -decay calculations

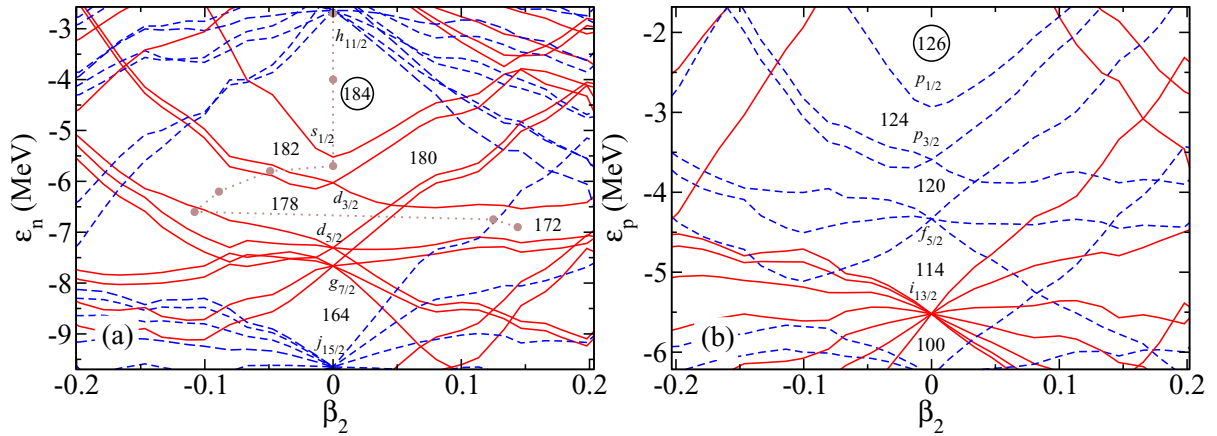


FIG. 8. (Color online) Nilsson diagrams for neutron levels (a) and proton levels (b) in  $^{298}\text{Fl}_{184}$ , obtained with SLy4. The large dots connected by a dotted line show the ground-state deformations of even-even  $_{114}\text{Fl}$  isotopes.

is employed. The ground states for the odd- $A$  nuclei are found by quasiparticle blocking in the equal filling approximation.

Figure 8 shows Nilsson diagrams for neutron and proton single-particle energies for  $^{298}\text{Fl}_{184}$  obtained with SLy4. Ground-state properties obtained from the calculations are summarized in Tables VI–VIII. Nuclei with  $N \geq 178$  are found to be near-spherical ( $|\beta| \leq 0.1$ ), whereas the lighter isotopes are deformed.

For the predicted near-spherical nuclei microscopic  $\alpha$ -decay calculations are performed in the same way as in the previous section but using the theoretical  $Q_{\text{gs-gs}}^{\text{th}}$  values and gs configurations. The odd quasiparticle states used in the spherical  $\alpha$ -decay calculation are selected by tracing the deformed states back to their spherical origin and picking the corresponding  $j$  shell. Figures 9 and 10 show the resulting gs-gs half-lives. The microscopic  $\alpha$ -decay half-lives are shown as solid lines. The dashed lines show the reference half-lives  $T_{\text{ref}}$ , Eq. (25), giving a hindrance factor  $\text{HF} = 1$ , obtained with the theoretical  $Q_{\text{gs-gs}}^{\text{th}}$  values. We have checked that these reference half-lives do not differ much from half-lives obtained from two semiempirical formulas [30,31] when the same  $Q_{\alpha}$  values are used. The largest difference for all considered superheavy nuclei is a factor 1.74 between  $T_{\text{ref}}$  and the UDL formula of Ref. [30], fitted to gs-gs  $\alpha$  decay of even-even nuclei. For the Viola-Seaborg formula fitted to heavy even-even nuclei in Ref. [31], the largest difference is a factor 16.2. This Viola-Seaborg formula consistently gives longer half-lives than  $T_{\text{ref}}$ , with the largest differences for the heaviest nuclei.

The predicted gs-gs half-lives for even- $Z$  isotope chains in Fig. 9 show a maximum at  $N = 183$ , caused by a minimum of the  $Q_{\alpha}$  value related to the  $N = 184$  shell closure (cf. Fig. 8). In the microscopic calculations, these half-lives are enhanced by hindrance as the odd neutron orbital changes from  $s_{1/2} \rightarrow d_{3/2}$ . Hindered gs-gs decay is also predicted for  $N = 185$  and for  $N = 179$ . For  $N = 185$  there is a change in parity of the mother and daughter ground states  $h_{11/2} \rightarrow s_{1/2}$ , and a large centrifugal barrier from the change in spin of the mother and daughter nucleus. The gs-gs decays of  $N = 179$  isotones are predicted to be hindered by a spin flip  $d_{3/2} \rightarrow d_{5/2}$ . These nuclei are close to the nuclei reached by current

experiments. The competition between the gs-gs decay and  $\alpha$  decay populating the excited  $d_{3/2}$  state in the daughter nucleus is investigated in Sec. VIC.

For the gs-gs decay of odd- $Z$  superheavy nuclei shown in Fig. 10, the decays of  $107_{182}$ ,  $109_{180,182}$ ,  $113_{184,186}$ , and  $115_{180}$  are predicted to be hindered. For the unfavored gs-gs decays of  $Z = 107$  and  $Z = 109$  isotopes the hindrance is from a change of the odd proton orbital  $i_{13/2}$  to  $f_{7/2}$ , which have different parities but the same orientation of the intrinsic spin. For the unfavored gs-gs decays of  $Z = 113, 115$  isotopes, the hindrance is associated with crossing the  $Z = 114$  gap, cf. Fig. 8. The odd proton orbital changes  $f_{5/2} \rightarrow i_{13/2}$ , implying both a change in parity and a spin flip. This gives a large hindrance, as seen by the large peaks in the microscopic  $T_{\text{gs-gs}}$  compared to the reference half-lives  $T_{\text{ref}}$  in Fig. 10. Note that in the results of the SHFB calculations, the ground state in  $113_{180,182,184,186}$  is predicted as a blocked quasiparticle state originating from the  $f_{5/2}$  shell, with the states originating from  $i_{13/2}$  at small excitation energies. The  $Z = 114$  gap seen in Fig. 8 is quite small, about 1.2 MeV for  $^{298}\text{Fl}_{184}$ . Blocking of an  $f_{5/2}$  quasiparticle gives in the calculations a larger pairing contribution to the binding energy than blocking an  $i_{13/2}$  quasiparticle, lowering the  $f_{5/2}$  state relative to the  $i_{13/2}$  state. If the effective pairing interaction strength is reduced, the ordering of these configurations is reversed, with states originating from  $i_{13/2}$  as the ground state, making the gs-gs decay of the mother nuclei  $115_{182,184,186}$  hindered instead.

### C. Competing decay channels

The gs-gs partial  $\alpha$ -decay half-life  $T_{\text{gs-gs}}$  gives an upper limit to the total  $\alpha$ -decay half-life  $T$ . Expressing  $T$  in terms of the widths  $\Gamma_k$  for the different  $\alpha$ -decay channels for a nucleus in its ground state gives

$$T = \frac{\hbar \ln(2)}{\Gamma_{\text{gs-gs}}(Q_{\text{gs-gs}}) + \sum_i \Gamma_{\text{gs-}i}(Q_{\text{gs-gs}} - E_i)}, \quad (33)$$

where  $Q_{\text{gs-gs}}$  is the gs-gs decay energy, and  $E_i$  denotes the excitation energy of excited state  $i$  in the daughter nucleus. For an even-even nucleus or when the gs-gs decay of an odd

TABLE VI. Predicted ground-state-to-ground-state (gs-gs)  $\alpha$ -decay properties of odd- $N$  superheavy nuclei. The  $Q_{\text{gs-gs}}$  value and the quadrupole deformation of the mother(daughter) nucleus  $\beta_{M(D)}$  are obtained in the axially deformed Skyrme-HFB calculations. gs  $M(D)$  denotes the asymptotic Nilsson quantum numbers  $2j\pi[N n_z \Lambda]$  of the blocked quasiparticle in the ground state of the mother(daughter) nucleus. 1-q.-p. states show the quasiparticle states used in the spherical microscopic  $\alpha$ -decay calculation.  $T_{\text{gs-gs}}$  is the gs-gs partial  $\alpha$ -decay half-life in seconds and  $\bar{\gamma}_{\text{gs-gs}}^2(r_t)$  the reduced width in MeV predicted by the microscopic  $\alpha$ -decay calculations.

$Z$	$N$	gs $M$	gs $D$	$\beta_M$	$\beta_D$	$Q_{\text{gs-gs}}$	$T_{\text{gs-gs}}$	$\bar{\gamma}_{\text{gs-gs}}^2(r_t)$	1-q.-p. states	Group
108	173	1+ [6 1 1]	1+ [6 1 1]	0.141	0.175	7.737				
108	175	3+ [6 4 2]	1+ [6 1 1]	-0.129	0.140	7.260				
108	177	1+ [6 4 0]	3+ [6 4 2]	-0.111	-0.130	6.805				
108	179	3+ [6 5 1]	1+ [6 4 0]	-0.077	-0.111	6.806	$4.322 \times 10^{10}$	$1.200 \times 10^{-4}$	$\nu : d_{3/2} \rightarrow d_{5/2}$	SF
108	181	3+ [6 0 2]	3+ [6 5 1]	0.011	-0.077	6.708	$2.234 \times 10^9$	$6.520 \times 10^{-3}$	$\nu : d_{3/2} \rightarrow d_{3/2}$	Fav
108	183	1+ [6 0 0]	3+ [6 0 2]	-0.000	0.011	5.951	$9.074 \times 10^{14}$	$1.978 \times 10^{-4}$	$\nu : s_{1/2} \rightarrow d_{3/2}$	SF
108	185	11-[7 0 5]	1+ [6 0 0]	-0.019	-0.000	8.049	$8.685 \times 10^5$	$2.551 \times 10^{-5}$	$\nu : h_{11/2} \rightarrow s_{1/2}$	PC
110	173	1+ [6 1 1]	1+ [6 1 1]	0.140	0.174	8.478				
110	175	15-[7 0 7]	1+ [6 1 1]	0.118	0.141	8.232				
110	177	1+ [6 4 0]	3+ [6 4 2]	-0.109	-0.129	7.509				
110	179	3+ [6 5 1]	1+ [6 4 0]	-0.076	-0.111	7.539	$1.628 \times 10^8$	$1.065 \times 10^{-4}$	$\nu : d_{3/2} \rightarrow d_{5/2}$	SF
110	181	3+ [6 0 2]	3+ [6 5 1]	0.011	-0.077	7.392	$1.314 \times 10^7$	$5.183 \times 10^{-3}$	$\nu : d_{3/2} \rightarrow d_{3/2}$	Fav
110	183	1+ [6 0 0]	3+ [6 0 2]	0.000	0.011	6.703	$6.016 \times 10^{11}$	$1.791 \times 10^{-4}$	$\nu : s_{1/2} \rightarrow d_{3/2}$	SF
110	185	11-[7 0 5]	1+ [6 0 0]	-0.019	-0.000	8.823	$1.129 \times 10^4$	$2.127 \times 10^{-5}$	$\nu : h_{11/2} \rightarrow s_{1/2}$	PC
112	173	1+ [6 1 1]	1+ [6 1 1]	0.137	0.168	9.142				
112	175	15-[7 0 7]	1+ [6 1 1]	0.118	0.140	9.077				
112	177	1+ [6 4 0]	15-[7 0 7]	-0.106	0.118	8.354				
112	179	3+ [6 5 1]	1+ [6 4 0]	-0.073	-0.109	8.236	$1.838 \times 10^6$	$9.767 \times 10^{-5}$	$\nu : d_{3/2} \rightarrow d_{5/2}$	SF
112	181	3+ [6 0 2]	3+ [6 5 1]	0.010	-0.076	8.059	$1.510 \times 10^5$	$5.177 \times 10^{-3}$	$\nu : d_{3/2} \rightarrow d_{3/2}$	Fav
112	183	1+ [6 0 0]	3+ [6 0 2]	-0.000	0.011	7.477	$1.047 \times 10^9$	$1.675 \times 10^{-4}$	$\nu : s_{1/2} \rightarrow d_{3/2}$	SF
112	185	11-[7 0 5]	1+ [6 0 0]	-0.019	0.000	9.605	$2.077 \times 10^2$	$2.179 \times 10^{-5}$	$\nu : h_{11/2} \rightarrow s_{1/2}$	PC
112	187	11-[7 0 5]	11-[7 0 5]	-0.017	-0.019	9.501	$1.378 \times 10^0$	$6.140 \times 10^{-3}$	$\nu : h_{11/2} \rightarrow h_{11/2}$	Fav
114	173	1+ [6 1 1]	1+ [6 1 1]	0.133	0.161	9.870				
114	175	15-[7 0 7]	1+ [6 1 1]	0.115	0.137	9.915				
114	177	1+ [6 4 0]	15-[7 0 7]	-0.102	0.118	9.243				
114	179	3+ [6 5 1]	1+ [6 4 0]	-0.070	-0.106	8.925	$4.074 \times 10^4$	$8.718 \times 10^{-5}$	$\nu : d_{3/2} \rightarrow d_{5/2}$	SF
114	181	3+ [6 0 2]	3+ [6 5 1]	0.010	-0.073	8.726	$3.847 \times 10^3$	$4.066 \times 10^{-3}$	$\nu : d_{3/2} \rightarrow d_{3/2}$	Fav
114	183	1+ [6 0 0]	3+ [6 0 2]	-0.000	0.010	8.273	$4.214 \times 10^6$	$1.491 \times 10^{-4}$	$\nu : s_{1/2} \rightarrow d_{3/2}$	SF
114	185	11-[7 0 5]	1+ [6 0 0]	-0.019	-0.000	10.414	$5.922 \times 10^0$	$1.996 \times 10^{-5}$	$\nu : h_{11/2} \rightarrow s_{1/2}$	PC
114	187	11-[7 0 5]	11-[7 0 5]	-0.016	-0.019	10.182	$8.229 \times 10^{-2}$	$5.495 \times 10^{-3}$	$\nu : h_{11/2} \rightarrow h_{11/2}$	Fav
116	173	1+ [6 1 1]	1+ [6 1 1]	0.126	0.154	10.750				
116	175	15-[7 0 7]	1+ [6 1 1]	0.110	0.133	10.791				
116	177	1+ [6 4 0]	15-[7 0 7]	-0.098	0.115	10.014				
116	179	3+ [6 5 1]	1+ [6 4 0]	-0.066	-0.102	9.683	$8.879 \times 10^2$	$7.830 \times 10^{-5}$	$\nu : d_{3/2} \rightarrow d_{5/2}$	SF
116	181	3+ [6 0 2]	3+ [6 5 1]	0.009	-0.070	9.508	$5.379 \times 10^1$	$4.059 \times 10^{-3}$	$\nu : d_{3/2} \rightarrow d_{3/2}$	Fav
116	183	1+ [6 0 0]	3+ [6 0 2]	0.000	0.010	9.165	$1.609 \times 10^4$	$1.531 \times 10^{-4}$	$\nu : s_{1/2} \rightarrow d_{3/2}$	SF
116	185	11-[7 0 5]	1+ [6 0 0]	-0.018	-0.000	11.260	$2.148 \times 10^{-1}$	$1.829 \times 10^{-5}$	$\nu : h_{11/2} \rightarrow s_{1/2}$	PC
116	187	11-[7 0 5]	11-[7 0 5]	-0.016	-0.019	10.923	$4.747 \times 10^{-3}$	$4.903 \times 10^{-3}$	$\nu : h_{11/2} \rightarrow h_{11/2}$	Fav
118	173	1+ [6 1 1]	1+ [6 1 1]	0.114	0.146	11.806				
118	175	3+ [6 4 2]	1+ [6 1 1]	-0.109	0.126	11.569				
118	177	1+ [6 4 0]	15-[7 0 7]	-0.093	0.110	10.708				
118	179	3+ [6 5 1]	1+ [6 4 0]	-0.062	-0.098	10.591	$1.239 \times 10^1$	$6.997 \times 10^{-5}$	$\nu : d_{3/2} \rightarrow d_{5/2}$	SF
118	181	3+ [6 0 2]	3+ [6 5 1]	0.008	-0.066	10.413	$7.506 \times 10^{-1}$	$3.203 \times 10^{-3}$	$\nu : d_{3/2} \rightarrow d_{3/2}$	Fav
118	183	1+ [6 0 0]	3+ [6 0 2]	-0.000	0.009	10.090	$1.453 \times 10^2$	$1.202 \times 10^{-4}$	$\nu : s_{1/2} \rightarrow d_{3/2}$	SF
118	185	11-[7 0 5]	1+ [6 0 0]	-0.018	0.000	12.148	$9.418 \times 10^{-3}$	$1.683 \times 10^{-5}$	$\nu : h_{11/2} \rightarrow s_{1/2}$	PC
118	187	11-[7 0 5]	11-[7 0 5]	-0.015	-0.018	11.728	$2.668 \times 10^{-4}$	$4.417 \times 10^{-3}$	$\nu : h_{11/2} \rightarrow h_{11/2}$	Fav
120	173	5+ [6 4 2]	1+ [6 1 1]	-0.117	0.133	12.528				
120	175	3+ [6 4 2]	1+ [6 1 1]	-0.103	0.114	12.179				
120	177	1+ [6 2 0]	3+ [6 4 2]	-0.083	-0.109	11.762				
120	179	3+ [6 5 1]	1+ [6 4 0]	-0.055	-0.093	11.678	$9.978 \times 10^{-2}$	$7.464 \times 10^{-5}$	$\nu : d_{3/2} \rightarrow d_{5/2}$	SF
120	181	3+ [6 0 2]	3+ [6 5 1]	0.006	-0.062	11.399	$9.318 \times 10^{-3}$	$3.291 \times 10^{-3}$	$\nu : d_{3/2} \rightarrow d_{3/2}$	Fav
120	183	1+ [6 0 0]	3+ [6 0 2]	0.000	0.008	11.115	$1.162 \times 10^0$	$1.197 \times 10^{-4}$	$\nu : s_{1/2} \rightarrow d_{3/2}$	SF
120	185	11-[7 0 5]	1+ [6 0 0]	-0.016	-0.000	13.083	$4.844 \times 10^{-4}$	$1.556 \times 10^{-5}$	$\nu : h_{11/2} \rightarrow s_{1/2}$	PC
120	187	11-[7 0 5]	11-[7 0 5]	-0.014	-0.018	12.654	$1.196 \times 10^{-5}$	$3.940 \times 10^{-3}$	$\nu : h_{11/2} \rightarrow h_{11/2}$	Fav

TABLE VII. Similar to Table VI, but for odd-proton superheavy nuclei.

$Z$	$N$	gs $M$	gs $D$	$\beta_M$	$\beta_D$	$Q_{\text{gs-gs}}$	$T_{\text{gs-gs}}$	$\tilde{\gamma}_{\text{gs-gs}}^2(r_t)$	1-q.-p. states	Group
107	172	1-[5 2 1]	9+ [6 2 4]	0.159	0.195	7.776				
107	174	1-[5 2 1]	1-[5 2 1]	0.133	0.164	7.180				
107	176	1-[5 0 1]	1-[5 0 1]	-0.121	-0.143	6.607				
107	178	1-[5 0 1]	1-[5 0 1]	-0.100	-0.121	6.471				
107	180	1-[5 1 0]	1-[5 0 1]	-0.065	-0.098	6.453	$1.390 \times 10^{10}$	$7.764 \times 10^{-3}$	$\pi : f_{7/2} \rightarrow f_{7/2}$	Fav
107	182	13+ [6 0 6]	1-[5 1 0]	0.003	-0.062	5.973	$4.138 \times 10^{15}$	$1.115 \times 10^{-5}$	$\pi : i_{13/2} \rightarrow f_{7/2}$	PC
107	184	13+ [6 0 6]	13+ [6 0 6]	0.001	-0.002	6.095	$1.208 \times 10^{12}$	$6.896 \times 10^{-3}$	$\pi : i_{13/2} \rightarrow i_{13/2}$	Fav
107	186	13+ [6 0 6]	13+ [6 0 6]	0.001	-0.001	7.717	$2.064 \times 10^4$	$7.888 \times 10^{-3}$	$\pi : i_{13/2} \rightarrow i_{13/2}$	Fav
109	172	3-[5 1 2]	9+ [6 2 4]	0.165	0.199	8.827				
109	174	1-[5 5 0]	1-[5 2 1]	0.129	0.159	7.913				
109	176	5-[5 3 2]	1-[5 2 1]	-0.119	0.133	7.391				
109	178	5-[5 0 3]	1-[5 0 1]	-0.100	-0.121	7.214				
109	180	5+ [6 2 2]	1-[5 0 1]	-0.063	-0.100	7.235	$1.417 \times 10^{10}$	$9.479 \times 10^{-6}$	$\pi : i_{13/2} \rightarrow f_{7/2}$	PC
109	182	13+ [6 0 6]	1-[5 1 0]	0.008	-0.065	6.701	$4.590 \times 10^{12}$	$9.053 \times 10^{-6}$	$\pi : i_{13/2} \rightarrow f_{7/2}$	PC
109	184	13+ [6 0 6]	13+ [6 0 6]	0.005	0.003	6.873	$8.786 \times 10^8$	$6.214 \times 10^{-3}$	$\pi : i_{13/2} \rightarrow i_{13/2}$	Fav
109	186	13+ [6 0 6]	13+ [6 0 6]	0.004	0.001	8.416	$3.347 \times 10^2$	$7.142 \times 10^{-3}$	$\pi : i_{13/2} \rightarrow i_{13/2}$	Fav
111	172	3-[5 1 2]	3-[5 1 2]	0.156	0.195	9.329				
111	174	11+ [6 1 5]	3-[5 1 2]	0.132	0.165	8.533				
111	176	5-[5 3 2]	1-[5 5 0]	-0.116	0.129	8.451				
111	178	5-[5 0 3]	5-[5 3 2]	-0.095	-0.119	7.841				
111	180	5-[5 0 3]	5-[5 0 3]	-0.063	-0.100	7.832	$4.813 \times 10^5$	$5.370 \times 10^{-3}$	$\pi : f_{5/2} \rightarrow f_{5/2}$	Fav
111	182	13+ [6 0 6]	5+ [6 2 2]	0.013	-0.063	7.394	$2.614 \times 10^7$	$6.294 \times 10^{-3}$	$\pi : i_{13/2} \rightarrow i_{13/2}$	Fav
111	184	13+ [6 0 6]	13+ [6 0 6]	0.008	0.008	7.690	$1.353 \times 10^6$	$6.238 \times 10^{-3}$	$\pi : i_{13/2} \rightarrow i_{13/2}$	Fav
111	186	13+ [6 0 6]	13+ [6 0 6]	0.008	0.005	9.131	$8.413 \times 10^0$	$6.382 \times 10^{-3}$	$\pi : i_{13/2} \rightarrow i_{13/2}$	Fav
113	172	3-[5 1 2]	3-[5 1 2]	0.148	0.182	9.876				
113	174	3-[5 1 2]	3-[5 1 2]	0.129	0.156	9.480				
113	176	7-[5 0 3]	11+ [6 1 5]	0.102	0.132	9.450				
113	178	1+ [6 3 1]	5-[5 3 2]	-0.093	-0.116	8.576				
113	180	5-[5 0 3]	5-[5 0 3]	-0.053	-0.095	8.502	$9.267 \times 10^3$	$4.656 \times 10^{-3}$	$\pi : f_{5/2} \rightarrow f_{5/2}$	Fav
113	182	5-[5 0 3]	5-[5 0 3]	-0.011	-0.063	8.133	$1.800 \times 10^5$	$5.204 \times 10^{-3}$	$\pi : f_{5/2} \rightarrow f_{5/2}$	Fav
113	184	5-[5 0 3]	13+ [6 0 6]	-0.006	0.013	8.388	$4.744 \times 10^7$	$2.023 \times 10^{-6}$	$\pi : f_{5/2} \rightarrow i_{13/2}$	PC SF
113	186	5-[5 0 3]	13+ [6 0 6]	-0.006	0.008	9.695	$1.972 \times 10^3$	$2.576 \times 10^{-6}$	$\pi : f_{5/2} \rightarrow i_{13/2}$	PC SF
115	172	1-[5 1 0]	1-[5 1 0]	0.142	0.172	10.437				
115	174	1-[5 1 0]	3-[5 1 2]	0.125	0.148	10.235				
115	176	3-[5 3 2]	3-[5 1 2]	-0.107	0.129	10.209				
115	178	3-[5 0 1]	7-[5 0 3]	-0.089	0.102	9.180				
115	180	3-[5 0 1]	1+ [6 3 1]	-0.051	-0.093	9.215	$3.637 \times 10^5$	$2.367 \times 10^{-6}$	$\pi : f_{5/2} \rightarrow i_{13/2}$	PC SF
115	182	5-[5 0 3]	5-[5 0 3]	-0.005	-0.053	8.778	$5.592 \times 10^3$	$4.081 \times 10^{-3}$	$\pi : f_{5/2} \rightarrow f_{5/2}$	Fav
115	184	5-[5 0 3]	5-[5 0 3]	-0.003	-0.011	9.103	$3.711 \times 10^2$	$4.603 \times 10^{-3}$	$\pi : f_{5/2} \rightarrow f_{5/2}$	Fav
115	186	5-[5 0 3]	5-[5 0 3]	-0.003	-0.006	10.350	$7.267 \times 10^{-2}$	$4.702 \times 10^{-3}$	$\pi : f_{5/2} \rightarrow f_{5/2}$	Fav
117	172	7-[5 0 3]	1-[5 1 0]	0.135	0.158	11.494				
117	174	1-[5 1 0]	1-[5 1 0]	0.111	0.142	11.377				
117	176	3-[5 3 2]	1-[5 1 0]	-0.101	0.125	10.862				
117	178	3-[5 0 1]	3-[5 3 2]	-0.081	-0.107	9.993				
117	180	3-[5 1 2]	3-[5 0 1]	-0.040	-0.089	10.049	$2.951 \times 10^0$	$4.137 \times 10^{-3}$	$\pi : f_{5/2} \rightarrow f_{5/2}$	Fav
117	182	5-[5 0 3]	3-[5 0 1]	0.002	-0.051	9.544	$8.659 \times 10^1$	$4.064 \times 10^{-3}$	$\pi : f_{5/2} \rightarrow f_{5/2}$	Fav
117	184	5-[5 0 3]	5-[5 0 3]	0.001	-0.005	10.081	$2.094 \times 10^0$	$4.071 \times 10^{-3}$	$\pi : f_{5/2} \rightarrow f_{5/2}$	Fav
117	186	5-[5 0 3]	5-[5 0 3]	0.001	-0.003	11.219	$2.195 \times 10^{-3}$	$4.201 \times 10^{-3}$	$\pi : f_{5/2} \rightarrow f_{5/2}$	Fav
119	172	1-[5 3 0]	7-[5 0 3]	-0.123	0.150	12.780				
119	174	1-[5 0 1]	7-[5 0 3]	-0.108	0.135	12.216				
119	176	1-[5 0 1]	1-[5 1 0]	-0.095	0.111	11.343				
119	178	1-[5 0 1]	3-[5 3 2]	-0.074	-0.101	11.076				
119	180	1-[5 4 1]	3-[5 0 1]	-0.040	-0.081	11.017	$3.670 \times 10^{-2}$	$3.736 \times 10^{-3}$	$\pi : f_{5/2} \rightarrow f_{5/2}$	Fav
119	182	5-[5 0 3]	3-[5 1 2]	0.009	-0.040	10.690	$2.344 \times 10^{-1}$	$3.703 \times 10^{-3}$	$\pi : f_{5/2} \rightarrow f_{5/2}$	Fav
119	184	5-[5 0 3]	5-[5 0 3]	0.005	0.002	11.196	$1.171 \times 10^{-2}$	$3.691 \times 10^{-3}$	$\pi : f_{5/2} \rightarrow f_{5/2}$	Fav
119	186	5-[5 0 3]	5-[5 0 3]	0.005	0.001	12.284	$3.913 \times 10^{-5}$	$3.790 \times 10^{-3}$	$\pi : f_{5/2} \rightarrow f_{5/2}$	Fav

TABLE VIII. Similar to Table VI, for even-even superheavy nuclei.

$Z$	$N$	$\beta_M$	$\beta_D$	$Q_{\text{gs-gs}}$	$T_{\text{gs-gs}}$	$\bar{\gamma}_{\text{gs-gs}}^2(r_i)$
108	172	0.160	0.192	8.214		
108	174	0.130	0.162	7.562		
108	176	-0.119	-0.140	6.940		
108	178	-0.097	-0.119	6.821	$5.241 \times 10^8$	$8.666 \times 10^{-3}$
108	180	-0.059	-0.096	6.780	$8.201 \times 10^8$	$8.146 \times 10^{-3}$
108	182	-0.000	-0.059	6.231	$6.552 \times 10^{11}$	$6.844 \times 10^{-3}$
108	184	-0.000	-0.000	6.502	$1.914 \times 10^{10}$	$7.564 \times 10^{-3}$
108	186	-0.000	-0.000	8.088	$1.969 \times 10^3$	$7.774 \times 10^{-3}$
110	172	0.155	0.192	9.024		
110	174	0.130	0.160	8.338		
110	176	-0.116	0.130	7.852		
110	178	-0.095	-0.119	7.542	$2.572 \times 10^6$	$6.776 \times 10^{-3}$
110	180	-0.058	-0.097	7.510	$3.501 \times 10^6$	$6.285 \times 10^{-3}$
110	182	-0.000	-0.059	6.966	$9.449 \times 10^8$	$5.986 \times 10^{-3}$
110	184	-0.000	-0.000	7.263	$3.697 \times 10^7$	$6.081 \times 10^{-3}$
110	186	-0.000	-0.000	8.768	$5.023 \times 10^1$	$6.986 \times 10^{-3}$
112	172	0.150	0.184	9.580		
112	174	0.129	0.155	9.112		
112	176	-0.113	0.130	8.888		
112	178	-0.092	-0.116	8.235	$3.173 \times 10^4$	$5.917 \times 10^{-3}$
112	180	-0.054	-0.095	8.207	$3.487 \times 10^4$	$6.338 \times 10^{-3}$
112	182	-0.000	-0.058	7.668	$4.538 \times 10^6$	$6.130 \times 10^{-3}$
112	184	-0.000	-0.000	8.032	$1.457 \times 10^5$	$6.085 \times 10^{-3}$
112	186	-0.000	-0.000	9.456	$1.920 \times 10^0$	$6.226 \times 10^{-3}$
114	172	0.144	0.173	10.185		
114	174	0.125	0.150	9.925		
114	176	-0.108	0.129	9.779		
114	178	-0.089	-0.113	8.924	$7.270 \times 10^2$	$5.129 \times 10^{-3}$
114	180	-0.049	-0.092	8.905	$7.181 \times 10^2$	$5.577 \times 10^{-3}$
114	182	-0.000	-0.054	8.395	$4.228 \times 10^4$	$5.429 \times 10^{-3}$
114	184	-0.000	-0.000	8.846	$9.904 \times 10^2$	$5.460 \times 10^{-3}$
114	186	-0.000	-0.000	10.160	$9.579 \times 10^{-2}$	$5.587 \times 10^{-3}$
116	172	0.136	0.164	11.032		
116	174	0.117	0.144	10.823		
116	176	-0.104	0.125	10.485		
116	178	-0.084	-0.108	9.663	$1.635 \times 10^1$	$5.078 \times 10^{-3}$
116	180	-0.042	-0.089	9.681	$1.379 \times 10^1$	$4.909 \times 10^{-3}$
116	182	-0.000	-0.049	9.199	$4.113 \times 10^2$	$4.838 \times 10^{-3}$
116	184	-0.000	-0.000	9.713	$9.700 \times 10^0$	$4.848 \times 10^{-3}$
116	186	-0.000	-0.000	10.945	$4.260 \times 10^{-3}$	$4.986 \times 10^{-3}$
118	172	0.121	0.153	12.120		
118	174	0.104	0.136	11.863		
118	176	-0.099	0.117	11.051		
118	178	-0.078	-0.104	10.580	$2.393 \times 10^{-1}$	$4.033 \times 10^{-3}$
118	180	-0.035	-0.084	10.599	$2.081 \times 10^{-1}$	$3.821 \times 10^{-3}$
118	182	-0.000	-0.042	10.122	$3.872 \times 10^0$	$3.805 \times 10^{-3}$
118	184	-0.000	-0.000	10.625	$1.542 \times 10^{-1}$	$3.816 \times 10^{-3}$
118	186	-0.000	-0.000	11.762	$2.282 \times 10^{-4}$	$4.495 \times 10^{-3}$
120	172	-0.123	0.138	12.728		
120	174	-0.106	0.121	12.396		
120	176	-0.090	0.104	11.744		
120	178	-0.067	-0.099	11.815	$9.086 \times 10^{-4}$	$4.174 \times 10^{-3}$
120	180	0.000	-0.078	11.755	$1.211 \times 10^{-3}$	$3.956 \times 10^{-3}$
120	182	-0.000	-0.035	11.084	$4.427 \times 10^{-2}$	$3.872 \times 10^{-3}$
120	184	-0.000	-0.000	11.557	$3.031 \times 10^{-3}$	$3.870 \times 10^{-3}$
120	186	-0.000	-0.000	12.682	$1.086 \times 10^{-5}$	$3.958 \times 10^{-3}$

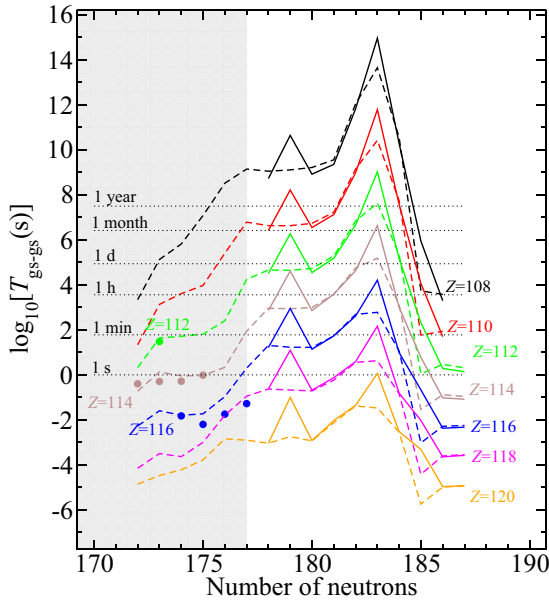


FIG. 9. (Color online) Ground-state-to-ground-state half-lives for even-even and even-odd superheavy isotopes. The dashed lines correspond to a hindrance factor  $HF = 1$ ; the solid lines are from the microscopic calculations with SLy4 and mixed pairing. The dots show available experimental data. The shaded area marks where the mother nuclei ground states are well deformed  $|\beta| \gtrsim 0.1$ .

nucleus is favored the gs-gs channel often dominates over the other  $\alpha$ -decay channels,  $\Gamma_{\text{gs-gs}}(Q_{\text{gs-gs}}) \gg \sum_i \Gamma_{\text{gs-}i}(Q_{\text{gs-gs}} - E_i)$ , giving  $T \approx \hbar \ln(2) / \Gamma_{\text{gs-gs}}$ . This is from the large sensitivity of the decay widths to the decay energy in combination with smaller formation amplitudes for unfavored channels.

For several odd- $A$  nuclei studied in the preceding subsection the gs-gs channel is unfavored, and the  $\alpha$  decay populating an excited state can dominate. We consider the favored excited state where the odd nucleon remains in the same orbital. The decay to the excited state relative the ground state depends on the hindrance factor and the excitation energy. The competition

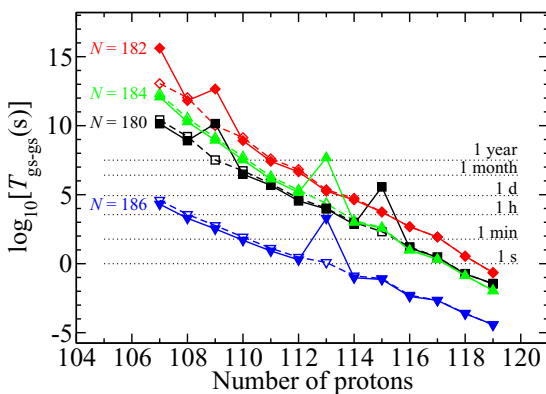


FIG. 10. (Color online) Similar to Fig. 9, but for even-even and odd-even superheavy nuclei, where the predicted mother and daughter nucleus deformation  $|\beta| \leq 0.1$ . Solid symbols connected by solid lines show the microscopic results; open symbols and dashed lines show half-lives corresponding to  $HF = 1$ .

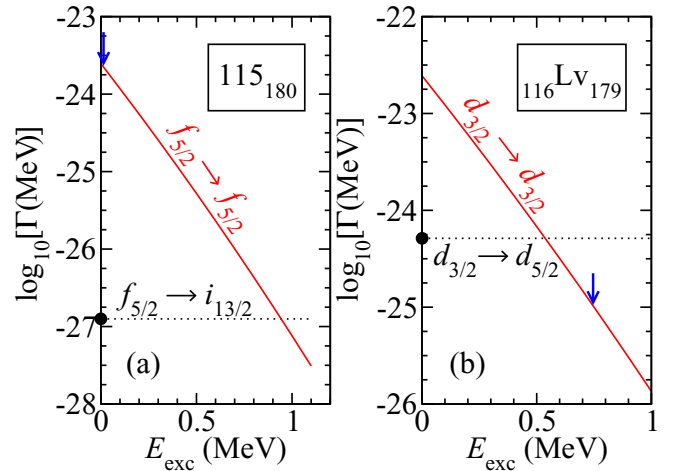


FIG. 11. (Color online) Competition between  $\alpha$ -decay channels for (a)  $115_{180}$ , and (b)  $116\text{Lv}_{179}$ . The black dots shows the predicted decay widths of the unfavored gs-gs decays. The red lines show the predicted decay width for the favored gs-es decay as a function of the excitation energy  $E_{\text{exc}}$  of the daughter nucleus where the odd nucleon remains in the same orbital as in the mother nucleus. The blue vertical arrows show the excitation energies of these states obtained in the HFB calculation.

between these two  $\alpha$ -decay channels is illustrated in Fig. 11. Figure 11(a) shows the predicted decay width for  $\alpha$  decay of  $115_{180}$  in its calculated  $f_{5/2}$  ground state to either the calculated ground state  $i_{13/2}$  of the daughter nucleus or the first excited  $f_{5/2}$  state at an excitation energy  $E_{\text{exc}}$ . Figure 11(b) shows a similar predicted competition between unfavored gs-gs decay and favored gs-es decay of  $116\text{Lv}_{179}$ .

For  $115_{180}$ , the predicted  $Q_{\text{gs-gs}} = 9.215$  MeV is obtained in the calculations described in Sec. VI B. The  $Q_{\text{gs-es}}$  value for decay populating the excited  $f_{5/2}$  state is set to  $Q_{\text{gs-es}} = Q_{\text{gs-gs}} - E_{\text{exc}}$ , where the excitation energy  $E_{\text{exc}}$  is varied. In this example the reduced width for the favored  $f_{5/2} \rightarrow f_{5/2}$  transition is a factor 1972 larger than for the unfavored, corresponding to a large hindrance. In the deformed calculations (Sec. VI B) the excitation energy of the first excited state is 14 keV. From Fig. 11 we see that the  $\alpha$  decay would be dominated by the favored decay channel populating the excited state. SHFB predictions for this excitation energy carry a large uncertainty. The intersection of the solid and dotted lines in Fig. 11 indicates that the favored  $\alpha$ -decay channel would dominate for an excitation energy of the favored state up to 0.9 MeV. Considering the high multipolarity and the low energy of possible  $\gamma$  decays, the predicted low-lying  $f_{5/2}$  excited state is likely to be isomeric with respect to  $\gamma$  decay, and will in turn decay by  $\alpha$  decay.

A similar analysis is made for  $116\text{Lv}_{179}$ . The predicted gs is a quasiparticle occupying a  $d_{3/2}$  orbital, while the predicted gs in the daughter nucleus  $114\text{Fl}_{177}$  originates from  $d_{5/2}$ . The  $d_{3/2}$  state in  $114\text{Fl}_{177}$  is predicted to have excitation energy 0.75 MeV. In this case the unfavored gs-gs  $\alpha$  decay dominates over the favored decay, giving no possibility for a subsequent  $\gamma$  decay. The  $\alpha$ -decay half-life is on the other hand hindered by

a factor  $\sim 50$  compared to the neighboring even-even nuclei, shown by the peak in the half-lives in Fig. 9.

From the intersection of the solid and dotted lines in Fig. 11(b), one can see that the unfavored gs-gs decay dominates if the excitation energy of the  $d_{3/2}$  state is larger than about 0.5 MeV. For the  $N = 179$  isotones studied in Sec. VIB, the ratio of the reduced width for the favored  $d_{3/2} \rightarrow d_{3/2}$  decay  $\bar{\gamma}_{\text{fav}}^2(r_t)$ , and the gs-gs decay  $\bar{\gamma}_{\text{gs-gs}}^2(r_t)$  is

$$\frac{\bar{\gamma}_{\text{fav}}^2(r_t)}{\bar{\gamma}_{\text{gs-gs}}^2(r_t)} = \{52.3, 50.6, 49.6, 48.6, 47.7, 46.7, 45.9\},$$

for  $Z = \{108, 110, 112, 114, 116, 118, 120\}$ , respectively. For these cases the slope of the decay width as a function of energy becomes flatter with increasing  $Z$ . The excitation energy where the more energetic gs-gs channel dominates increases from 0.34 MeV for  $108_{179}$  to 0.65 MeV for  $120_{179}$ .

The competition between favored and hindered  $\alpha$ -decay channels illustrated here depends on a balance of the hindrance factor and the  $Q$ -value dependence of the Coulomb penetrability. The hindrance factors depend strongly on the orbitals of the odd nucleons, so to make detailed predictions each  $\alpha$ -decaying odd nucleus needs to be considered separately. In general, the slope of the decay width as a function of energy is flatter for superheavy nuclei than for medium-mass nuclei, because of the scaling of the penetrability with proton number and  $Q$  value. Also, in general the density of single-particle levels increases when the mass increases. This should lead to on the average smaller excitation energies for the states in the daughter nuclei where the odd nucleon remains in the same orbital. These two observations lead to the general conclusion that the favored decay to a suitable excited state should be the dominant  $\alpha$ -decay channel more often for superheavy nuclei than for medium-mass nuclei.

Superheavy nuclei can  $\alpha$  decay in several steps before the  $\alpha$ -decay chain is ended by spontaneous fission. In each  $\alpha$ -decay step there is a competition between  $\alpha$ -decay channels. For a sufficiently long  $\alpha$ -decay chain, one cannot expect that the odd nucleon will remain in the same orbital in all the nuclei of the chain. Considering the above example of  $115_{180}$ ,  $\alpha$ -decay populating a low-lying excited state in the daughter nucleus  $113_{178}$ , where the odd proton remains in the same  $f_{5/2}$  orbital, is predicted to be the dominant decay channel. In the subsequent  $\alpha$  decay of  $113_{178}$  there is again a competition between a favored  $f_{5/2} \rightarrow f_{5/2}$  channel where the odd proton remains in the same orbital, but where the excitation energy of the favored state is larger, and a channel with a larger  $Q_\alpha$  value where the odd proton changes orbital. At some point along the chain the odd nucleon will change orbital, either through  $\gamma$  decay or by  $\alpha$  decay through an unfavored channel with a larger  $Q_\alpha$  value, as in the example of  ${}_{116}\text{Lv}_{179}$ , shown in the second panel of Fig. 11.

#### D. Discussion on ground-state and $Q_\alpha$ predictions

The particle numbers where one can expect hindered gs-gs  $\alpha$  decay depend on the ordering of the single-particle levels. The size of the gaps in the spherical single-particle spectra can differ significantly in different self-consistent mean-field models [14,32]. However, the models compared in Ref. [32]

all predict the same ordering for neutron and proton spherical shells in this mass region as SLy4, with a few exceptions: The order of the  $j_{13/2}$  and the  $h_{11/2}$  neutron shells above  $N = 184$  is reversed in some models. For protons shells below  $Z = 114$ , some of the models get  $f_{7/2}$  above the  $i_{13/2}$  shell.

The SHFB calculations do not consider beyond-mean-field corrections to the binding energy. The effect on  $Q_\alpha$  values should be quite small, except near the spherical  $N = 184$  shell closure, where the magnitude of the correction varies quickly with particle number [14]. Calculations with a relativistic mean-field approach combined with a collective Hamiltonian for even-even superheavy nuclei in the  $\alpha$ -decay chain of  $120_{178,180}$  were reported in Ref. [33]. The effect of symmetry restoration and quadrupole vibrations on the  $Q_\alpha$  values was found to be small, at most  $\sim 0.5$  MeV for the deformed  $Z = 112, 114$  isotopes. In the generator coordinate method calculations presented in Ref. [14], the effect on  $Q_\alpha$  values was also observed to be small, except near  $N = 184$ . The  $Q_\alpha$  values of the even-even  $N = 184$  isotones with  $Z \geq 120$  are increased by up to around 1 MeV when beyond-mean-field correlations are included. For the nuclei  $120_{183,184,185}$  we can thus expect that the half-life predicted by the calculations presented here is overestimated by up to two orders of magnitude. For the remaining nuclei, we expect the effect on the half-life to be small.

## VII. SUMMARY AND OUTLOOK

Microscopic calculations for the  $\alpha$ -particle formation and  $\alpha$ -decay half-lives were performed for near-spherical odd- $A$  nuclei. An  $R$ -matrix-type microscopic formalism was used for the calculation of the decay rate, using HFB wave functions obtained with the SLy4 Skyrme effective interaction and different pairing prescriptions as inputs for the calculation of the formation amplitude. Following the method of our previous study [15] the reduced widths were renormalized with a single mass-independent scaling factor fitted to even-even nuclei.

The obtained decay rates reproduced the available data for  $\alpha$  decay of near-spherical odd- $A$  nuclei well. The variation in the reduced widths of both favored and hindered decays were reasonably described in the calculations. The root-mean-square deviation of the logarithm of the theoretical decay rate from the corresponding experimental value was 0.68–0.79, depending on the effective pairing interaction used. If three pathological cases out of the 45 studied cases are removed from consideration the RMS is reduced to 0.39–0.44, i.e., the calculated decay rates are correct within a factor 3.

The studied cases were classified according to how the orbital of the odd nucleon changes in the  $\alpha$  decay. Comparing favored and unfavored  $\alpha$  decays there is a clear difference in the reduced widths and hindrance factors. The variation of the hindrance factors for different unfavored decays was large, and could not be described by a simple selection rule. To predict hindrance factors detailed calculations must indeed be performed.

After the test of the method on decays where experimental data exist, the approach was applied to ground-state-to-ground-state  $\alpha$  decay of near-spherical superheavy nuclei. Based on  $Q_\alpha$  values and level structure obtained in deformed

HFB calculations, we predict the longest  $\alpha$ -decay half-lives for  $N = 183$  isotones. The partial half-lives of gs-gs transitions of  $N = 179, 183$ , and  $185$  isotones, as well as  $Z = 113$  and  $115$  isotopes are enhanced by hindrance. These nuclei are candidates for higher probability of  $\alpha$ -decay populating excited states in the daughter nucleus and thus giving rise to subsequent  $\gamma$  decay.

The adopted approach works well for describing the relative decay rates of both odd- $A$  and even-even nuclei. By extending the method to deformed HFB states, the approach may offer a practical method of predicting relative rates and hindrance factors across the nuclear chart.

As future experiments on superheavy nuclei move up in the nuclear chart and possibly reach the near-spherical region, the gs-gs  $\alpha$  decays will be hindered when there is a change of  $j$  shells for the odd particle. The hindrance factor depends on the shell structure. If the gs-gs decay or a favored decay to an excited state is observed depends on the hindrance factor and the energy distance between shells. If the decay populates an excited state, consecutive  $\gamma$  decay can give further information on the shell structure. The approach presented here then offers a possibility to study in detail the competition of different possible  $\alpha$ -decay scenarios, suggested by the data and nuclear structure models.

### ACKNOWLEDGMENTS

D. Rudolph is acknowledged for inspiring discussions on superheavy nuclei, and for suggesting studies of possible hindered gs-gs  $\alpha$  decay. B.G.C. and S.Å. thank the Swedish Research Council (VR) for financial support.

### APPENDIX A: $\alpha$ -PARTICLE WAVE FUNCTION

We employ the following model  $\alpha$ -particle wave function [16],

$$\begin{aligned} \Phi_{00}^{(\alpha)}(\mathbf{r}_\pi, \mathbf{r}_\nu, \mathbf{r}_\alpha, s_1, s_2, s_3, s_4) \\ = \left( \frac{4}{b_\alpha^3 \sqrt{\pi}} \right)^{3/2} e^{-\frac{r_\pi^2 + r_\nu^2 + r_\alpha^2}{2b_\alpha^2}} \left( \frac{1}{\sqrt{4\pi}} \right)^3 \\ \times [\chi_{\frac{1}{2}}(s_1), \chi_{\frac{1}{2}}(s_2)]_{00} [\chi_{\frac{1}{2}}(s_3), \chi_{\frac{1}{2}}(s_4)]_{00}, \end{aligned} \quad (\text{A1})$$

with the oscillator length  $b_\alpha = 1.42$  fm. We use the Jacobi coordinates  $\mathbf{r}_\pi, \mathbf{r}_\nu, \mathbf{r}_\alpha, \mathbf{R}_\alpha$  related to the laboratory coordinates  $\mathbf{r}_1, \mathbf{r}_2, \mathbf{r}_3, \mathbf{r}_4$  of the valence particles through:

$$\begin{pmatrix} \mathbf{r}_\pi \\ \mathbf{r}_\nu \\ \mathbf{r}_\alpha \\ \mathbf{R}_\alpha \end{pmatrix} = \frac{1}{2} \begin{pmatrix} \sqrt{2} & -\sqrt{2} & 0 & 0 \\ 0 & 0 & \sqrt{2} & -\sqrt{2} \\ 1 & 1 & -1 & -1 \\ 1 & 1 & 1 & 1 \end{pmatrix} \begin{pmatrix} \mathbf{r}_1 \\ \mathbf{r}_2 \\ \mathbf{r}_3 \\ \mathbf{r}_4 \end{pmatrix}. \quad (\text{A2})$$

The formation amplitude  $g_{kL_\alpha}$  defined in the coordinates (A2) is related to the formation amplitude  $f_{kL_\alpha}$  defined for the physical separation of the centers of mass  $r$  as [34]

$$f_{kL}(r) = \sqrt{8} g_{kL}(2r). \quad (\text{A3})$$

### APPENDIX B: TWO-PARTICLE TRANSFER AMPLITUDES

For the spherical symmetric HFB vacua used here the quasiparticle creation operator can be written,

$$\beta_{nljm}^\dagger = \sum_{n'} U_{n'n}^{lj} a_{n'ljm}^\dagger - (-1)^{j-m} V_{n'n}^{lj} a_{n'lj-m}, \quad (\text{B1})$$

where  $a_{n'ljm}^\dagger$  creates a particle in the spherical oscillator state with  $n'$  radial nodes, orbital angular momentum  $l$ , total angular momentum  $j$ , and angular momentum projection  $m$ .  $n$  labels the quasiparticles corresponding to the same  $l$  and  $j$  in order of increasing energy.  $U_{n'n}^{lj}$  and  $V_{n'n}^{lj}$  correspond to matrix elements of the HFB  $U$  and  $V$  matrices [35].

The formation amplitude (12) depends on the four-particle transfer amplitudes,

$$\langle D_{00} | \beta_{k_D I_D M_D}^D a_{\nu l} a_{\nu k} a_{\pi j} a_{\pi i} \beta_{k_M I_M}^{M\dagger} | M_{00} \rangle. \quad (\text{B2})$$

As p-n mixing is not considered we only need to consider the following overlaps, expressed in the spherical oscillator basis,

$$\langle D_0 | a_{\alpha' j' m'} a_{\alpha j m} | M_0 \rangle, \quad (\text{B3})$$

for the even-numbered particle species, and

$$\langle D_0 | \beta_{k_D I_D M_D}^D a_{\alpha' j' m'} a_{\alpha j m} \beta_{k_M I_M}^{M\dagger} | M_0 \rangle, \quad (\text{B4})$$

for the odd-numbered particle species. To save space the labeling  $\alpha \equiv (nl)$  is used.  $|M_0\rangle$  ( $|D_0\rangle$ ) is the relevant particle-species part of the mother(daughter) HFB vacuum.

Expanding  $|M_0\rangle$  in terms of  $|D_0\rangle$  with Thouless' theorem and using the generalized Wick theorem, the overlaps can be written in terms of three different two-particle transfer densities [35]. The first is

$$\begin{aligned} \kappa_{\alpha j m, \alpha' j' m'}^{(\text{DM})*} &= \frac{\langle M_0 | a_{\alpha j m}^\dagger a_{\alpha' j' m'}^\dagger | D_0 \rangle}{\langle M_0 | D_0 \rangle} \\ &= \delta_{jj'} \delta_{m, -m'} (-1)^{j-m} \kappa_{\alpha, \alpha'}^{(\text{DM})j*}. \end{aligned} \quad (\text{B5})$$

This density is the only one needed for the even-numbered particle species. The other two densities are

$$\begin{aligned} \kappa_{\alpha j m, \alpha' j' m'}^{(\text{MD})} &= \frac{\langle M_0 | a_{\alpha' j' m'} a_{\alpha j m} | D_0 \rangle}{\langle M_0 | D_0 \rangle} \\ &= \delta_{jj'} \delta_{m, -m'} (-1)^{j-m} \kappa_{\alpha, \alpha'}^{(\text{MD})j}, \end{aligned} \quad (\text{B6})$$

and

$$\rho_{\alpha j m, \alpha' j' m'}^{(\text{MD})} = \frac{\langle M_0 | a_{\alpha' j' m'}^\dagger a_{\alpha j m} | D_0 \rangle}{\langle M_0 | D_0 \rangle} = \delta_{jj'} \delta_{mm'} \rho_{\alpha, \alpha'}^{(\text{MD})j}. \quad (\text{B7})$$

The transfer densities for the odd-numbered particle species can now be computed,

$$\begin{aligned} \langle D_0 | M_0 \rangle^{-1} \langle D_0 | \beta_{k_D I_D M_D}^D a_{\alpha' j' m'} a_{\alpha j m} \beta_{k_M I_M}^{M\dagger} | M_0 \rangle \\ = +\delta_{I, I_D} \delta_{M M_D} \delta_{j' j} \delta_{m', -m} (-1)^{j-m} \kappa_{\alpha, \alpha'}^{(\text{DM})j} F_{k_D, k_M} \\ - \delta_{I j} \delta_{M m} \delta_{I_D j'} \delta_{M_D, -m'} (-1)^{I_D - M_D} H_{\alpha, k_M; \alpha', k_D} \\ + \delta_{I j'} \delta_{M m'} \delta_{I_D j} \delta_{M_D, -m} (-1)^{I_D - M_D} H_{\alpha', k_M; \alpha, k_D}, \end{aligned} \quad (\text{B8})$$

where the  $F$  coefficient is given by

$$\begin{aligned} F_{k_D, k_M} = & (U^{(D)I\dagger}(1 - \rho^{(MD)I})^\dagger U^{(M)I})_{k_D, k_M} + (V^{(D)I\dagger} \rho^{(MD)I*} V^{(M)I})_{k_D, k_M} \\ & + (U^{(D)I\dagger} \kappa^{(DM)I, T} V^{(M)I})_{k_D, k_M} + (V^{(D)I\dagger} \kappa^{(MD)I*} U^{(M)I})_{k_D, k_M}, \end{aligned} \quad (B9)$$

and the  $H$  coefficient by

$$H_{\alpha, k_M; \alpha', k_D} = ((\kappa^{(DM)I, T} V^{(M)I})_{\alpha, k_M} + ((1 - \rho^{(MD)I})^\dagger U^{(M)I})_{\alpha, k_M}) ((\kappa^{(DM)I, D} U^{(D)I, D*})_{\alpha', k_D} + (\rho^{(MD)I, D} V^{(D)I, D*})_{\alpha', k_D}). \quad (B10)$$

### Expressions for the BCS case

Considering a standard seniority pairing BCS calculation the expressions for the transfer amplitudes become simpler. The same spherical single-particle basis is used for the mother and daughter nucleus. The BCS wave function can be expressed in terms of quasiparticles of the form (B1) with the  $U$  and  $V$  matrices  $U_{n'n}^{lj} = \delta_{nn'} u_{nlj}$ , and  $V_{n'n}^{lj} = \delta_{nn'} (-1)^l v_{nlj}$ .

The expression for the overlap of vacua then becomes

$$|\langle D_0 | M_0 \rangle|^2 = \prod_{lj} \prod_a (u_{alj}^D u_{alj}^M + v_{alj}^D v_{alj}^M)^{2j+1}, \quad (B11)$$

and for the two-particle transfer amplitudes,

$$\kappa_{aa'}^{(DM)lj*} = \delta_{aa'} u_{alj}^D (u_{alj}^D u_{alj}^M + v_{alj}^D v_{alj}^M)^{-1} (-1)^l v_{alj}^M, \quad (B12)$$

$$F_{aa'} = \delta_{aa'} (u_{alj}^D u_{alj}^M + v_{alj}^D v_{alj}^M)^{-1}, \quad (B13)$$

$$H_{\alpha, k_M; \alpha', k_D} = \delta_{\alpha k_M \alpha' k_D} \delta_{\alpha' k_D} u_{k_M l_M j_M}^D v_{k_D l_D j_D}^M (-1)^{l_D} (u_{k_M l_M j_M}^D u_{k_M l_M j_M}^M + v_{k_M l_M j_M}^D v_{k_M l_M j_M}^M)^{-1} (u_{k_D l_D j_D}^D u_{k_D l_D j_D}^M + v_{k_D l_D j_D}^D v_{k_D l_D j_D}^M)^{-1}. \quad (B14)$$

- 
- [1] S. G. Nilsson *et al.*, *Nucl. Phys. A* **131**, 1 (1969).  
 [2] E. O. Fiset and J. R. Nix, *Nucl. Phys. A* **193**, 647 (1972).  
 [3] A. Staszczak, A. Baran, and W. Nazarewicz, *Phys. Rev. C* **87**, 024320 (2013).  
 [4] M. Leino and F. P. Heßberger, *Ann. Rev. Nucl. Part. Sci.* **54**, 175 (2004).  
 [5] D. Rudolph *et al.*, *Phys. Rev. Lett.* **111**, 112502 (2013).  
 [6] *Alpha-, Beta-, and Gamma-Ray Spectroscopy*, edited by K. Seigbahn (North-Holland, Amsterdam, 1965), Vol. 1.  
 [7] G. T. Seaborg and W. D. Loveland, *The Elements beyond Uranium* (John Wiley & Sons, New York, 1990).  
 [8] H. J. Mang, *Phys. Rev.* **119**, 1069 (1960).  
 [9] H.-D. Zeh and H. J. Mang, *Nucl. Phys.* **29**, 529 (1962).  
 [10] H.-D. Zeh, *Z. Phys.* **175**, 490 (1963).  
 [11] J. K. Poggenburg, H. J. Mang, and J. O. Rasmussen, *Phys. Rev.* **181**, 1697 (1969).  
 [12] M. Bender, P.-H. Heenen, and P.-G. Reinhard, *Rev. Mod. Phys.* **75**, 121 (2003).  
 [13] S. Ćwiok, P.-H. Heenen, and W. Nazarewicz, *Nature (London)* **433**, 705 (2005).  
 [14] M. Bender and P.-H. Heenen, *J. Phys.: Conf. Ser.* **420**, 012002 (2013).  
 [15] D. E. Ward, B. G. Carlsson, and S. Åberg, *Phys. Rev. C* **88**, 064316 (2013).  
 [16] R. G. Lovas, R. J. Liotta, A. Insolia, K. Varga, and D. S. Delion, *Phys. Rep.* **294**, 265 (1998).  
 [17] D. S. Delion, *Theory of Particle and Cluster Emission*, Lecture Notes in Physics No. 819 (Springer, New York, 2010).  
 [18] D. E. Ward, B. G. Carlsson, and S. Åberg, *Phys. Scr.* **89**, 054027 (2014).  
 [19] E. Chabanat, P. Bonche, P. Haensel, J. Meyer, and R. Schaeffer, *Nucl. Phys. A* **635**, 231 (1998).  
 [20] M. V. Stoitsov, N. Schunck, M. Kortelainen, N. Michel, H. Nam, E. Olsen, J. Sarich, and S. Wild, *Comput. Phys. Commun.* **184**, 1592 (2013).  
 [21] B. G. Carlsson, J. Dobaczewski, J. Toivanen, and P. Veselý, *Comput. Phys. Commun.* **181**, 1641 (2010).  
 [22] G. P. Kamuntavičius, R. K. Kalinauskas, B. R. Barret, S. Mickevičius, and D. Germanas, *Nucl. Phys. A* **695**, 191 (2001).  
 [23] I. Tonzuka and A. Arima, *Nucl. Phys. A* **323**, 45 (1979).  
 [24] R. I. Betan and W. Nazarewicz, *Phys. Rev. C* **86**, 034338 (2012).  
 [25] K. Varga, R. G. Lovas, and R. J. Liotta, *Nucl. Phys. A* **550**, 421 (1992).  
 [26] K. Varga and R. J. Liotta, *Phys. Rev. C* **50**, R1292 (1994).  
 [27] P. Moller, J. R. Nix, W. D. Myers, and W. J. Swiatecki, *At. Data Nucl. Data Tables* **59**, 185 (1995).  
 [28] The ENSDF database, <http://www.nndc.bnl.gov/ensdf/> (2014).  
 [29] M. Samyn, S. Goriely, and J. M. Pearson, *Nucl. Phys. A* **725**, 69 (2003).  
 [30] C. Qi, F. R. Xu, R. J. Liotta, R. Wyss, M. Y. Zhang, C. Asawatangtrakuldee, and D. Hua, *Phys. Rev. C* **80**, 044326 (2009).  
 [31] A. Parkhomenko and A. Sobczewski, *Acta Phys. Pol. B* **36**, 3095 (2005).  
 [32] M. Bender, K. Rutz, P.-G. Reinhard, J. A. Maruhn, and W. Greiner, *Phys. Rev. C* **60**, 034304 (1999).  
 [33] V. Prassa, T. Nikšić, G. A. Lalazissis, and D. Vretenar, *Phys. Rev. C* **86**, 024317 (2012).  
 [34] J. Eichler and H.-J. Mang, *Z. Phys.* **183**, 321 (1965).  
 [35] P. Ring and P. Schuck, *The Nuclear Many-Body Problem*, 1st ed. (Springer-Verlag, New York, 1980).